Universidade de Aveiro Departamento de Química
Ano 2010

Vasyl Skrypnychuk

Preparação de células solares híbridas à base de P3HT, óxido de zinco e nanotubos de carbono

Fabrication of hybrid solar cells based on P3HT, zinc oxide and carbon nanotubes

Universidade de Aveiro Departamento de Química
Ano 2010

Vasyl Skrypnychuk

Preparação de células solares híbridas à base de P3HT, óxido de zinco e nanotubos de carbono

Fabrication of hybrid solar cells based on P3HT, zinc oxide and carbon nanotubes

Dissertation presented to University of Aveiro for the requirement of partial fulfilment of the Masters of Science degree in materials science under supervision of Dr. Ana Barros, Department of Chemistry of the University of Aveiro and Dr. António F. da Cunha, Department of Physics of the University of Aveiro.

Dissertação apresentada à Universidade de Aveiro para cumprimento dos requisitos necessários à obtenção do grau de Mestre em Ciência dos Materiais, realizada sob a orientação científica da Dra. Ana Barros Timmons, Professora Auxiliar do Departamento de Química da Universidade de Aveiro e do Dr. António F. da Cunha, Professor Auxiliar do Departamento de Fisica da Universidade de Aveiro.

o júri

Doutora Maria João de Sousa Brites, Investigadora Auxiliar, LNEG

Prof. Dra. Ana Barros Timmons, Prof. Auxiliar, Universidade de Aveiro

Prof. Dr. António F. da Cunha, Prof. Auxiliar, Universidade de Aveiro

Prof. Dr. rer. nat. Wolfgang Bauhofer, TUHH, Alemanha

acknowledgements

I am very thankful to my supervisors, Prof. Ana Barros Timmons and Prof. António F. da Cunha, for the opportunity of working in this fascinating field and for the permanent support that I have been obtaining from them.

I would also like to thank all the people who helped me to carry out the experiments, particularly Mr. Diogo Mata, Ms. Marta Ferro, Dr. Édison Pecoraro, Ms. Celeste Azevedo.

Finally, I thank the EMMS consortium for enabling the cultural and educational experience I have had over the last two years, and the European Commission for the financial support.

palavras-chave

célula fotovoltaica híbrida, P3HT, óxido de zinco, nanopartículas, ácido pireno-1- carboxílico, nanotubos de carbono

resumo

Recentemente tem-se vindo a registar um interesse significativo no estudo de células fotovoltaicas híbridas devido ao facto da tecnologia requerida para o ser simples e flexível, o que associado a uma eficiente capacidade de conversão da energia solar as tornará economicamente viáveis. A utilização de nanopartículas inorgânicas veio aumentar o potencial interesse neste campo já que os efeitos de confinamento quântico associados ao reduzido tamanho das partículas tem permitido aumentar a eficiência deste tipo de células.

Neste trabalho, foram estudadas células fotovoltaicas híbridas à base de poli(3-hexiltiofeno) (P3HT) e nanopartículas de ZnO. Utilizaram-se nanopartículas de ZnO com e sem modificação superficial com o ácido pireno-1-carboxílico (PCA). Adicionalmente foi ainda estudado o efeito de nanotubos de carbono (CNT) comerciais e de florestas de CNT preparadas por deposição química em fase vapor (CVD), sobre o comportamento dos nanocompósitos de P3HT/ZnO.

As nanopartículas de ZnO foram sintetizadas e caracterizadas por SEM, DLS e por espectroscopia no UV-Vis, no IV e de fotoluminescência.
A morfologia dos filmes compósitos de P3HT, nanopartículas de ZnO (modificadas ou não) e CNT (componentes da camada activa) foi analisada por SEM. Verificou-se que a modificação superficial das nanopartículas de ZnO com PCA levou a uma ligeira melhoria da sua dispersão na matriz de P3HT, nomeadamente no caso dos nanocompósitos contendo CNT. As propriedades ópticas destes materiais foram estudadas por espectroscopia no UV-Vis e de fotoluminescência.

As células solares híbridas foram preparadas com a seguinte configuração: Vidro/ITO/PEDOT:PSS/camada fotoactiva/Al. As suspensões de PEDOT:PSS bem como das camadas fotoactivas foram depositadas por *spin-coating* sobre um substrato de vidro revestido com ITO, sendo por fim depositada uma camada de alumínio por evaporação térmica.

A caracterização dos dispositivos foi feita através de medições de corrente-tensão sob condições simuladas de iluminação padrão. Apesar da adição de CNT ter levado a um aumento significativo da densidade de corrente, a maioria das células fotovoltaicas preparadas não apresentou actividade fotovoltaica.

Por fim, são discutidos possíveis factores que poderão ser responsáveis pelo desempenho insatisfatório dos dispositivos preparados e propostas algumas sugestões para trabalho futuro.

keywords hybrid solar cell, P3HT, zinc oxide, nanoparticles, pyrene-1-carboxylic acid, carbon nanotubes

abstract

An ever growing interest is now focused on the development of hybrid solar cells as potentially cheap, easy and efficient technology for solar energy conversion.
Specifically, the application of inorganic nanoparticles for this purpose can boost cell efficiency due to the particle size-related effects.

In the present work, hybrid solar cells based on poly(3-hexylthiophene) (P3HT) and ZnO nanoparticles were investigated. Both unmodified and surface-modified with pyrene-1-carboxylic acid (PCA) nanoparticles of ZnO were used
Additionally, the effect of carbon nanotubes on the properties of P3HT/ZnO composites was tested. Both pristine and CVD-grown carbon nanotubes were applied.

ZnO nanoparticles were synthesized and characterized by SEM, DLS, and UV-Vis, photoluminescence and IR spectroscopies. The morphology of the films of different composites prepared using P3HT, ZnO nanoparticles and carbon nanotubes (active layer composites) was analyzed by SEM. Modification of ZnO nanoparticles with PCA lead to a slight improvement of their dispersion quality in P3HT which was further improved when carbon nanotubes were added to the P3HT / PCA-modified ZnO composite. The optical properties of the ensuing composite materials were studied by UV-Vis and photoluminescence spectroscopies.

The hybrid solar cells with the structure Glass/ITO/PEDOT:PSS/active layer composite/Al were prepared by successive spin-coating of the corresponding suspensions on ITO-coated glass substrates, followed by deposition of an aluminium layer by thermal evaporation. The current-voltage characteristics of the cells were measured under simulated standard illumination conditions. Although the addition of carbon nanotubes yielded a significant increase in current density, most of the cells did not show any photovoltaic effect.

Finally, possible factors responsible for the low efficiency of the cells prepared are discussed and some suggestions for future work are proposed.

CONTENTS

LIST OF FIGURES

List of abbreviations

°C	degrees centigrade
Al	aluminium
CB	conduction band
cm	centimetre(s)
CNT	carbon nanotubes
CVD	chemical vapour deposition
DLS	dynamic light scattering
DMSO	dimethyl sulphoxide
eV	electron-volt(s)
FT	Fourier transform
HOMO	highest occupied molecular orbital
IPCE	internal photon-to-current conversion efficiency
IR	infrared
ITO	indium tin oxide
kV	kilovolt(s)
LUMO	lowest unoccupied molecular orbital
M	mole(s) per litre
ml	millilitre(s)
mV	millivolt(s)
MWCNT	multi-walled carbon nanotubes
nm	nanometre(s)
NP	nanoparticle(s)
P3HT	poly(3-hexylthiophene)
P3OT	poly(3-octylthiophene)
PCA	pyrene-1-carboxylic acid
PCBM	[6,6]-phenyl-C61-butyric acid methyl esther
PEDOT:PSS	mixture of poly(3,4-ethylenedioxythiophene) and poly(styrenesulfonate)
PVD	physical vapour deposition
s	second(s)
sccm	standard cubic centimetres per minute
SEM	scanning electron microscope / scanning electron microscopy
STC	standard test conditions
STEM	scanning transmission electron microscope / scanning transmission electron microscopy
SWCNT	single-walled carbon nanotubes
TiO_2	titanium oxide
UV	ultraviolet
UV-Vis	ultraviolet-visible
UV-Vis-NIR	ultraviolet-visible-near-infrared

V	volt(s)
VB	valence band
W/m^2	watt(s) per square metre
X	times (image magnification)
ZnO	zinc oxide
ZnO@PCA	zinc oxide nanoparticles surface-functionalized with pyrene-1-carboxylic acid
ZnO FNP	zinc oxide nanoparticles surface-functionalized with pyrene-1-carboxylic acid
η	efficiency
µm	micrometre(s)

1. Introduction

Solar energy is the type of energy that can have the most universal application among all the energy sources known up-to-date. In fact, only 1/10000 of solar irradiation that reaches the surface of the Earth can provide all the electricity needed for mankind, if it is fully converted [1]. The power that can be obtained per square metre for solar energy equals about 170 W/m^2 depending on the geographical location and weather conditions. Though it is up to 10000 times lower than, for instance, in case of wind energy, solar panels meet virtually no restrictions for being mounted (e.g., they are safe, do not produce any noise), and thus they can be applied more universally, including integration into newly built roof and wall structures, as well as into already existing ones. As a consequence, this type of energy source seems to be very promising for the future of electricity generation.

The most mature solar cell technology utilizes thick silicon-based solar panels and it already finds a market. Though their efficiency is relatively high (up to 30% [2]), there are a number of economical aspects that make up a problem. First of all, a lot of energy is required in order to produce a thick silicon solar panel. The main process which consumes energy in this case is the production of silicon, as it has to be reduced from the natural form of silicon dioxide. As a consequence, the price of such a panel is relatively high and pay-off time is long as well. So the development of cheaper solar cells with reasonably high efficiency is required [1].

This requirement is met by thin-film solar technologies. The inorganic thin film solar cells already are sufficiently cheaper due to the low cost of production. Among the materials used for their production, one can name amorphous silicon, copper indium gallium selenide, copper indium selenide, cadmium telluride and some others [1].

Though all of these materials more or less fulfil the above mentioned pricing requirements, in many cases the solar cells made of them use a rigid substrate (e.g., glass), making the cells non-flexible. But flexibility is one of the key issues for switching to cheap production techniques like roll-to-roll production [3]. Besides, the perspective of further increasing of the efficiency of inorganic thin film solar cells is unclear, though research in this direction is being performed.

As a consequence, a lot of attention has been focused on the development of polymeric and hybrid solar cells.

The main advantage of using polymeric materials for solar energy conversion is that these materials are lightweight, they are flexible, have comparably low price (as very thin films are used for the production of the cell) and, as it was mentioned above, in principle there is a possibility of applying cheap roll-to-roll technologies for the production of large-area solar elements.

However, the major disadvantage at this moment is the low efficiency of solar energy conversion of organic cells compared to thin film cells based on inorganic semiconductor materials. For example, the maximum efficiency that has been reported for an organic cell based purely on organic materials is 7.9 % [4]. It has been proposed, that the reasonable efficiency for the cells to be sold on the market starts from about 10%. So research has to be done in order to achieve this goal.

The solar cell efficiency is dependent on a number of aspects, and various materials and device concepts have been used in order to improve it. Among these materials, organic-inorganic hybrids are very promising and, in general, the use of the intrinsic properties of the organic and inorganic components can be made, as well as the synergistic properties of the two components can arise. Consequently, the hybrid materials can be designed to enable efficient light-to-current conversion over a wide range of wavelengths of the solar spectrum and to improve charge transfer.

In brief, the main aims of this work are:

- to review the progress that has been made in this direction and to figure out possible ways of improving the efficiency of polymer-based solar cells;
- to produce hybrid solar cells based on one of the most common organic semiconductors, poly-3-hexylthiophene (P3HT), and zinc oxide nanostructures;
- to test the influence of the incorporation of carbon nanotubes into P3HT / zinc oxide hybrid solar cells on their efficiency and microstructure.

This work is organised in the following way: first, a literature review is presented, including some general issues on the structure and operation of organic and hybrid solar cells, as well as more specific considerations on the use of carbon nanotubes, zinc oxide and organic dyes in solar cells. Afterwards, the experimental part describes the materials, devices and practical methods used in the work. In the next chapter, the experimental results are presented and discussed. Finally, conclusions are drawn in the last chapter.

2. Literature review

2.1. Principle of organic and hybrid thin film solar cell operation

An organic thin film solar cell consists of two flat electrodes, one of which is transparent (the most common transparent electrode is indium tin oxide, ITO), and a photoactive layer in between (figure 1). This layer is made of light-absorbing organic semiconductor that absorbs all the electromagnetic radiation with energy higher than the energy of its band gap [5]. Absorption of light causes the formation of excitons, or electron-hole pairs, that further dissociate contributing to electron and hole currents to different electrodes (desired process) or recombine resulting in emission of energy in the form of light or heat (undesired). Typical organic semiconducting materials are conjugated polymers that also act as conductors of charge after the charges have been generated. Examples of the widely used conducting polymers are poly-3-hexylthiophene (P3HT); poly[2,1,3-benzothiadiazole-4,7-diyl[4,4-bis(2-ethylhexyl)-4H-cyclopenta[2,1-b:3,4-b']dithiophene-2,6-diyl]] (PCPDTBT); poly[2-methoxy-5-(2'-ethyl-hexyloxy)-1,4-phenylene vinylene] (MEH-PPV) (see the chemical structures on figure 2).

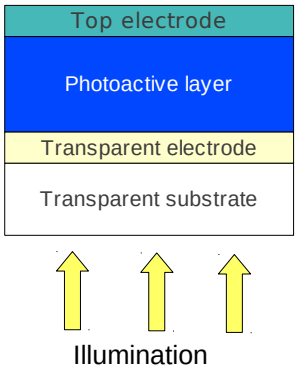

Figure 1. Schematic structure of an organic thin film solar cell.

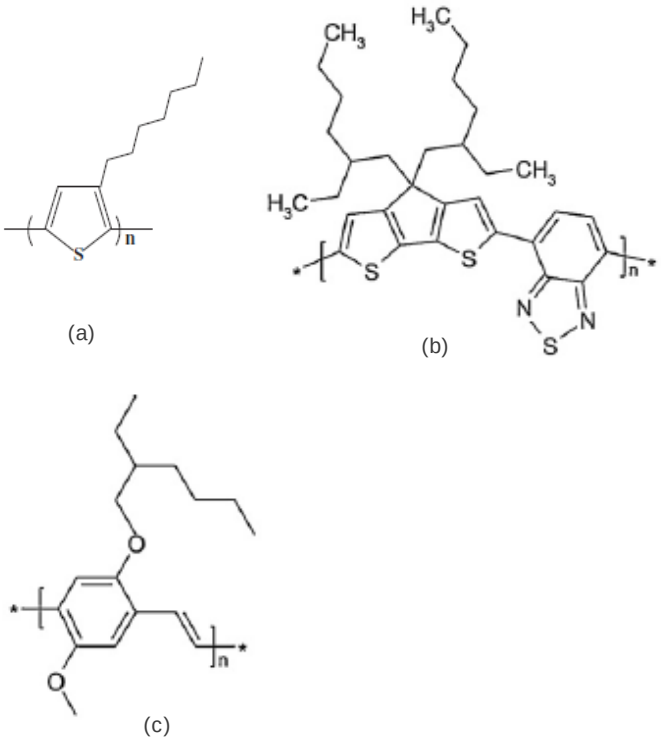

Figure 2. Chemical structures of (a) P3HT; (b) PCPDTBT; (c) MEH-PPV [5].

In order to increase the efficiency of the solar cell (i.e., the efficiency of light-to-current conversion), the exciton dissociation process needs to be efficient. This can be achieved by introducing electron-accepting materials into the organic semiconductor. One of the most popular class of organic acceptor materials are fullerene derivatives like [6,6]-phenyl-C61-butyric acid methyl esther (PCBM). Mixing of the organic semiconductors and organic acceptors leads to the formation of the so-called 'bulk heterojunction' design (figure 3). This kind of active layer architecture allows forming very thin alternating regions of donor and acceptor materials, reaching the values of the exciton diffusion length (i.e., the distance an exciton can travel without recombination, equalling 5-15 nm for most organic semiconductors [5]), hence enabling the excitons to efficiently dissociate at the junction of donor and acceptor materials and electrons and holes to be conducted through the acceptor and the donor, correspondingly. In fact, one of the highest up-to-date efficiencies of organic solar cells (6.77%, [7]) has been achieved using the bulk heterojunction concept with PCBM as an acceptor material and specially synthesized low-bandgap conjugated polymer, namely, a fluorine-substituted polymer poly[4,8-bis-substituted-benzo[1,2-b:4,5-b']dithiophene-2,6-diyl-alt-4-substituted-thieno[3,4-b] thiophene-2,6-diyl] (PBDTTT-CF, see the chemical structure on figure 4).

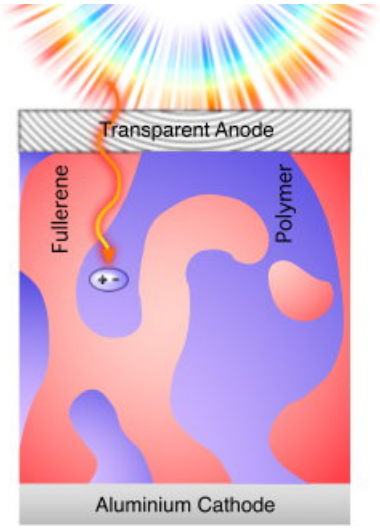

Figure 3. Sketch of bulk heterojunction morphology of the active layer [6].

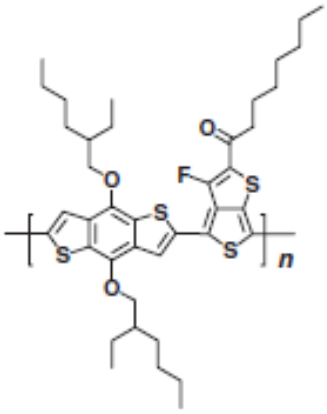

Figure 4. Chemical structure of PBDTTT-CF [7].

The other promising acceptors for organic semiconductor-based solar cells are inorganic semiconductors, especially nanosized ones [8]. Hence, this type of solar cells are called hybrid. Various kinds of inorganic semiconductors have been used in hybrid solar cells, including silicon, cadmium telluride, copper indium selenide, copper indium sulphide, cadmium selenide, cadmium sulphide, titanium oxide, zinc oxide and others [5]. Besides being an electron-accepting component, the inorganic semiconductors can contribute to the overall cell efficiency by their own absorption of light, the efficiency of which depends on the band gap value. And the nano-dimension of the inorganic materials is beneficial, first of all, due to the large total area of the nanoparticle/polymer interface; in addition, the specific nano-effects like the appearance of quantum wells or multi-exciton generation can occur in such type of an active layer material that can bring about improved cell efficiency [8]. The factors that determine the cell efficiency will be discussed in one of the next chapters.

The structure of the solar cell can also be represented in terms of the corresponding energy levels of its components. As an example, a typical organic solar cell which has a layer sequence glass/ITO/PEDOT:PSS/P3HT:PCBM/Al will possess an electronic structure represented on figure 6. Here, PEDOT:PSS stands for the mixture of poly(3,4-ethylenedioxythiophene) and poly(styrenesulfonate) (see the chemical structures on figure 5), and is used as a hole conducting material to improve the hole transfer from the photoactive layer (P3HT:PCBM) to the ITO, as well as the smoothness of the ITO surface.

Knowing the position of the energy levels of the materials that are intended to be used in a solar cell, it is possible to choose them properly and assure the high value of potential difference between the lowest unoccupied molecular orbital (LUMO) of the acceptor material (-3.7 eV for PCBM in this example case) and the highest occupied molecular orbital (HOMO) of the donor material (-5.2 eV for P3HT in this case), so that the electrons that have been formed at the P3HT/PCBM interface and have been withdrawn by PCBM, will have lower probability of recombination with the holes located at the HOMO of P3HT. Instead, there should be a higher probability for the electrons to flow in the direction of the anode and for the holes to flow in the direction of the cathode (see figure 5).

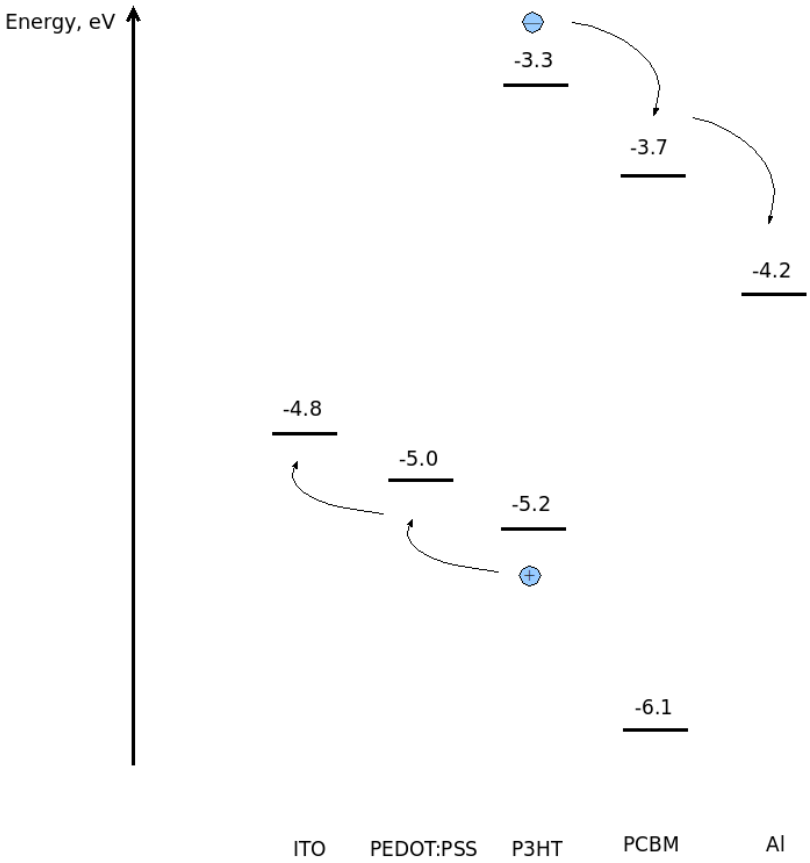

Figure 5. Energy level diagram of the ITO/PEDOT:PSS/P3HT:PCBM/Al solar cell.

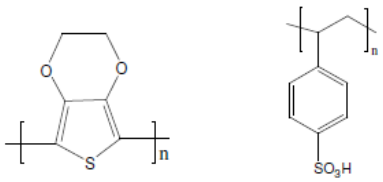

Figure 6. Chemical structures of PEDOT (left) and PSS (right) [9].

The rational choice of the components for the solar cell will be discussed in more detail in the following sub-chapters.

2.2. Determination of solar cell efficiency

The efficiency of a solar cell is practically assessed by measuring its current-voltage characteristics under simulated sun illumination (see figure 7). When a solar cell operates under illumination, the current density - voltage curve intersects the corresponding axes at zero resistance (short circuit) and infinite resistance (open circuit). The points of intersect are called the short circuit current density (J_{sc}) and open circuit voltage (U_{OC}), correspondingly. And at a certain point of the curve, the power density is the biggest, $P_{max} = U_{ph}^{max} \cdot J_{ph}^{max}$. This value determines the efficiency of the solar cell (η), if divided by the illumination power density (P_0):

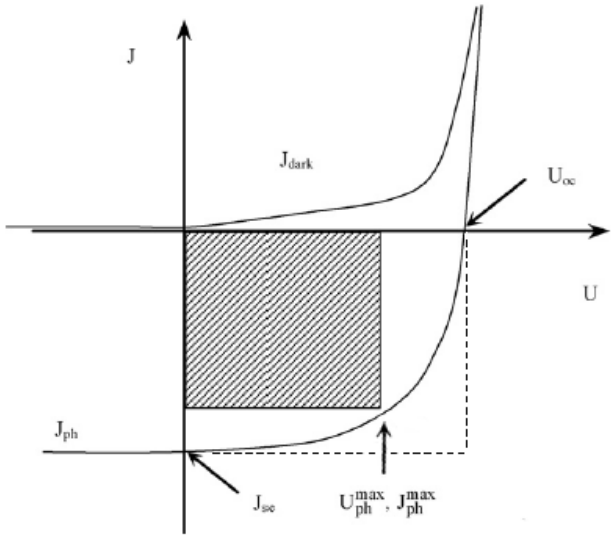

Figure 7. Current density versus applied voltage curves of a solar cell in dark and under illumination [5].

$$\eta = \frac{P_{max}}{P_0}$$

Another parameter that is widely used is the fill factor (*FF*), which characterizes the quality of a solar cell and can be determined as a ratio between the maximal power density of the cell (shadowed area) and the ideal power density in case of a square-like current-voltage curve (area shown by a dash line):

$$FF = \frac{P_{max}}{J_{SC} \cdot U_{OC}}$$

The above mentioned parameters should be measured at the standard test conditions (STC), namely the temperature of 25°C, illumination power 1000 W/m^2 and air mass 1.5 irradiation spectrum (defined by the American Society for Testing and Materials), that corresponds to the influence of the Earth atmosphere at 48.2° solar zenith angle.

2.3. Ways of improving the efficiency of organic and hybrid solar cells

In order to achieve high solar cell efficiency values, every single stage of light-to-current conversion needs to be efficient, because the overall efficiency can be calculated as a multiplication of all the efficiencies of the intermediate stages.

The factors that need to be taken into account can be divided into the following groups:

a) efficiency of light absorption and exciton generation, including:

→ proper solar spectrum coverage of the solar cell materials.

Photons of every wavelength of the solar spectrum (figure 8) need to be absorbed in the best efficiency solar cell for terrestrial application. According to the intensity distribution of the spectrum it has been shown that the best result for a single absorber is achieved when it possesses the semiconductor band gap of about 1.4 eV [10], that corresponds to the wavelength of about 885 nm. However, in this case some part of the energy is being lost as the IR region of the spectrum is not covered.

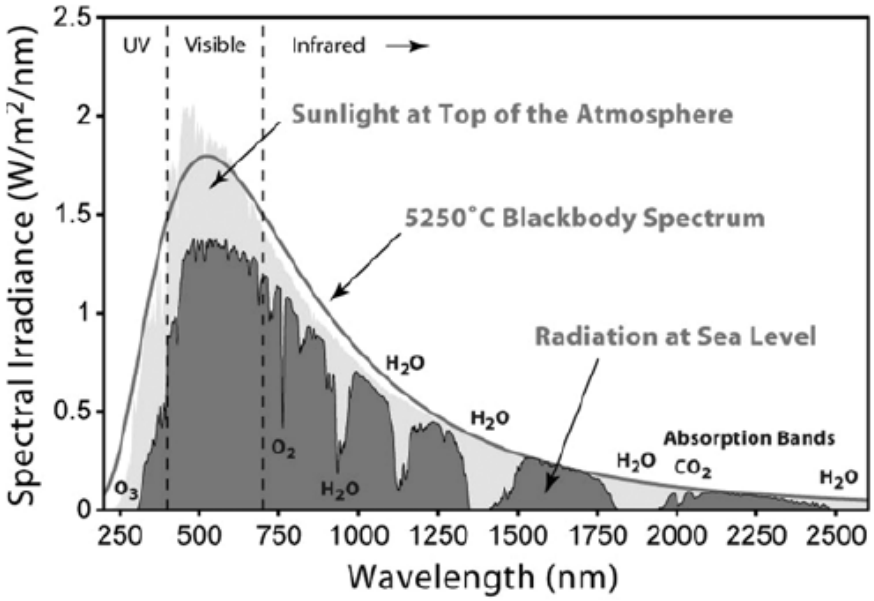

Figure 8. Solar spectrum at the top of the atmosphere (compared to the blackbody spectrum) and at sea level (with the designation of the atmospheric absorption bands) [1].

For P3HT as the sole absorber in the cell, the band gap equals 1.9 eV, so it can theoretically cover only 22.4% of the solar energy [11]. Hence, a popular approach when using a single absorbing material (in the case of organic solar cells) is tuning the band gap to be narrow enough to enable the absorption of most of the IR part of the spectrum, and the photons of higher energy at the same time. However, a disadvantage of this approach is that a big portion of energy is lost because the energy difference between the photon energy and the organic semiconductor band gap can only be converted into heat, and not into current (see the scheme on figure 9).

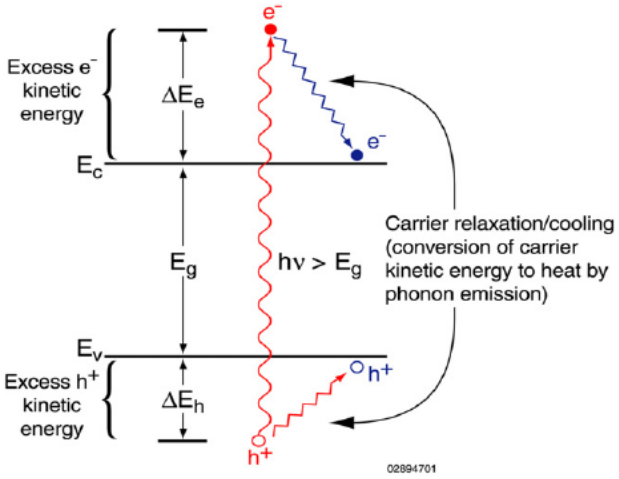

Figure 9. Scheme of energy losses caused by internal conversion [12].

As a consequence, a combination of materials with different bandgaps seems to be the optimal way, so that both the biggest intensity part in the visible region is efficiently absorbed and the IR-region is not lost. In 'classical' solar panels this approach is achieved by the production of multi-layered cells, where every next layer absorbs light with shorter wavelength than the previous one [1]. However, this approach limits the solar cell thickness and flexibility, so a different way could be mixing all the absorbers in one thin film composite material.

Solar spectrum coverage is one of the reasons for the incorporation of inorganic semiconductors and the development of hybrid solar cells. In this case, the semiconductor is chosen depending on the type of its electronic structure (direct band gap semiconductors are more efficient absorbers than indirect band gap ones) and on the band gap value. For example, a combination of an organic semiconductor with the band gap corresponding to the wavelength of the near-IR region and an inorganic

semiconductor with the band gap near the maximum of solar irradiation intensity should bring about efficient solar spectrum coverage. Examples of such semiconductors are GaAs, CdTe [5].

Another way to cover the solar spectrum is dye-sensitization of the inorganic component. According to this approach, the surface of the inorganic semiconductor is modified with an organic dye, the absorption spectrum of which is chosen so that it covers the needed part of the spectrum. As a result, the light absorbed by the dye contributes to the exciton generation that takes place inside of the inorganic semiconductor. Hence the inorganic material may start absorbing the light of the wavelengths that it was not capable to absorb before [5]. This is of great importance especially for the semiconductors absorbing in the short wavelength visible region, like ZnO or TiO_2, as it may be the way to boost the efficiency of solar cells which incorporate these inorganic semiconductors.

→ avoiding recombination and luminescence losses.

This requirement primarily addresses energy levels of the materials that are used, ensuring that the electrons and holes formed in the photoactive material can be separated and contribute to electron and hole flows to the corresponding electrodes.

According to this approach, the electrons/holes formed in the photoactive layer(s) need to be able to flow only to the materials that assure the pathway to a certain electrode, and not to the opposite ones. That is controlled by the relative location of the energy levels of the semiconductors and conductors present in the solar cell (see the previous sub-chapter, figure 5). The proper sequence of contacts between the materials has to assure that the energy barriers for the electrons/holes flow are minimal or absent.

If this requirement is not met then the probability of recombination of charges increases. Recombination may lead either to the production of heat or to the emission of photons (i.e., to luminescence losses).

→ proper exciton mobility and exciton dissociation efficiency.

Exciton diffusion length values are relatively low (about 5-15 nm [5]) for organic semiconductors, compared to the inorganic ones. Consequently, the morphology of the

active layer should be tuned up so that the thickness of the regions of donor polymer phase does not exceed this value. Hence, good dispersion quality of acceptor material in the donor one is required. That can be achieved, for example, via proper solvent choice, concentration, ratio of donor to acceptor, temperature and spin-coating parameters. Another interesting method is using block-copolymerisation, so that the different blocks of the polymer belong to the donor and acceptor phases, correspondingly. The latter method may enable very precise tuning of the phase thickness [13].

In addition, a prospective way of improving the morphology is the use of miniemulsion for the preparation of donor and acceptor nanocomposites [14], followed by mixing of them and destruction of the miniemulsion with the formation of the desired bulk heterojunction in the active layer.

b) efficiency of electron and hole transfer to the electrodes:

→ proper electron and hole mobility in the corresponding materials, i.e., high electron and hole conductivity. This is one of the main reasons for the use of inorganic components as charge mobility values of the inorganic semiconductors are much higher than those of polymeric semiconductors [5].

This is explained by the difference in molecular structure of organic and inorganic materials: electrons that are responsible for the conductivity are more localized in the case of organic semiconductors (in fact, the conductivity is the highest in the direction of the conjugation chain of the polymer) whereas in the case of an inorganic semiconductor the charge carriers mobility is not that restricted and is preformed through the crystalline lattice of the material;

→ existence of percolation, i.e., proper interface molecular design that avoids undesired ohmic losses at the interfaces. The ohmic losses correspond directly to the recombination that takes place at the interface.

The percolation has to be assured for the following interfaces:

* cathode / donor material of the photoactive layer
* donor material / acceptor material (to avoid losses during exciton dissociation)
* acceptor material / anode

Furthermore, percolation inside the donor material and inside the acceptor material needs to be present. In fact, absence of percolation seems to be the main reason for the poor carrier mobility in organic semiconductors. Even if there is no recombination during the electron/hole transfer through the conjugated chain of the polymer, losses are very likely to occur during the charge transfer between two different macromolecules. One of the possible mechanisms for the charge transfer in this case involves the formation of π-π-complexes between the aromatic rings of the different macromolecules (on the example of polythiophene-type polymeric semiconductors, figure 10), and the efficiency of this process is much lower, as it depends on the relative spatial location of the rings and the related steric effects.

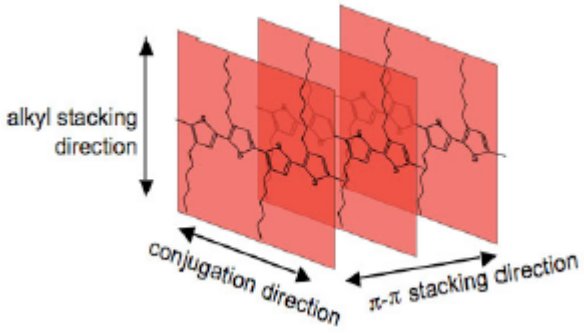

Figure 10. Mechanism of π-π-stacking in P3HT [15].

In case of the use of inorganic acceptor materials, percolation is also a crucial issue, because isolated particles are likely to contribute to the recombination losses, as the charges generated by light absorption or injected from the surrounding donor material have no way out of the particle but for being recombined.

c) stability of the solar cell operation, i.e., absence of its degradation with time.

In case of solar cells based on conjugated polymers like P3HT this becomes a big problem as the polymer oxidizes when exposed to air and/or humidity. Hence, the efficiency of the cell decreases significantly [13]. One way of avoiding such a degradation process is complete isolation of the material from the oxidizing media, like production of the solar cells in inert atmosphere with subsequent encapsulation. A different approach is the modification of the chemical structure of the polymeric semiconductor so that the structure of the polymer becomes non-susceptible to oxidation, for instance, by avoiding the relatively easy-oxidizable $-CH_2-$ and -CH=CH- groups in the structure of the polymer [13].

2.4. Use of carbon nanotubes in organic solar cells

Carbon nanotubes (CNT) are known for their outstanding mechanical and electronic conductivity properties. Even small amounts of CNT can increase the conductivity of a polymer-based CNT composite drastically ([16]-[18]).
In addition to the high conductivity values, normally a CNT sample contains a mixture of metallic (workfunction = - 4.5 – - 5.0 eV) and semiconducting (VB level = - 4.8 eV, CB level = - 5.4 eV) nanotubes [19]. Hence, when CNT are incorporated into the solar cell, some light absorption in the visible range can be expected due to the semiconductor component.

CNT have been applied for the modification of various layers of the solar cell [20]. Most of the works utilize direct mixing of CNT with the material of the active layer in a solar cell (e.g., with pure semiconducting polymers like P3HT or P3OT (poly(3-octylthiophene)) [21], or mixtures of donor and acceptor polymers, like the P3HT:PCBM bulk heterojunction mixture ([22]-[26])). Both single-walled carbon nanotubes (SWCNT) ([27], [28]) and multi-walled ones (MWCNT) ([22], [28]) have been used for these purposes.

Another approach is using CNT for the modification of the transparent conductive electrodes ([29]-[31]) or substitution of the conventional transparent conducting electrodes with carbon nanotube-based electrode ([32], [33]), as it can be a cheaper and more accessible material than ITO which is being widely used now. It can also help overcome the mechanical drawbacks of ITO [34]. Moreover, CNT are reported to have been used for the production of hole-ejecting layer, which conventionally is made of a hole conductor like PEDOT:PSS [35].

One of the major problems in the production of polymer/CNT composites using pristine CNT is the dispersion quality of CNT in the polymer matrix [36]. As a consequence of the strong van der Waals interaction between the CNT, they tend to form bundles and agglomerates if the polymer-CNT compatibility is low. This agglomeration may lead to the degradation of the desired properties, including mechanical and electrical.

Among the ways that have been applied in order to solve this problem, mechanical blending, chemical functionalization of the tubes and dispersant-assisted mixing have been used [16]. The first of these methods normally involves the use of ultrasonication and does not yield a stable dispersion, as the CNT re-agglomerate rapidly after being dispersed. The other two methods lead

to more stable systems, however, chemical treatment normally introduces changes to the electronic properties of the nanotubes and it also lowers their conductivity.

However, in CNT composite based on conjugated polymers an intrinsic dispersion mechanism may take place, namely π-π interaction between the π-system of the nanotubes and the aromatic rings of the polymer (figure 11). Besides good dispersion quality, this can bring about the formation of pathways for efficient electron transfer, that is also favourable for the solar cell operation.

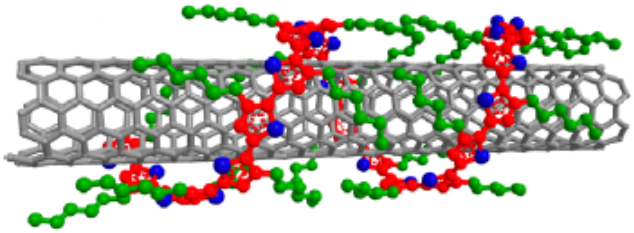

Figure 11. Mechanism of π-π interaction in CNT-P3HT composites [26].

In order to increase the contact area between the carbon nanotubes and the corresponding electrode (which is likely to be rather low because of the wrapping of the tubes with the conducting polymer), CNT can be seeded and grown directly on the desired substrate, forming aligned CNT arrays [37]. This aligned CNT arrays are reported to be grown by chemical vapour deposition (CVD) on various substrates [38], though no data of practical application of the aligned CNT arrays in solar cells has been reported.

In addition to the improvement of the contact between CNT and the substrate, another way of increasing the efficiency of the cell is via applying the 'bulk heterojunction' architecture, i.e., aligned CNT assure the high contact area between CNT and the adjacent semiconducting polymer. Consequently, CNT can improve the charge carrier transfer efficiency from the conducting polymer to the electrode where they were grown on.

2.5. Use of zinc oxide in hybrid excitonic solar cells

Zinc oxide is receiving an ever-growing attention due to its good electronic properties, namely: being a direct band gap semiconductor (therefore, it possesses high light absorption coefficient), relatively high electron mobility (200 $cm^2 \cdot V^{-1} \cdot s^{-1}$) and relatively high value of the valence band energy (of about 4.5 eV; in terms of band energy values, ZnO is very similar to another semiconductor, namely, TiO_2) [5], which in principle let ZnO be an efficient acceptor material by providing reasonably high values of the energetic barrier that gives rise to the open-circuit voltage of the solar cell (see scheme on figure 12). Besides, the transparency of ZnO and the possibility to prepare particles of different shapes via simple wet chemistry-based techniques ([39], [40]) are also important advantages for the use of ZnO.

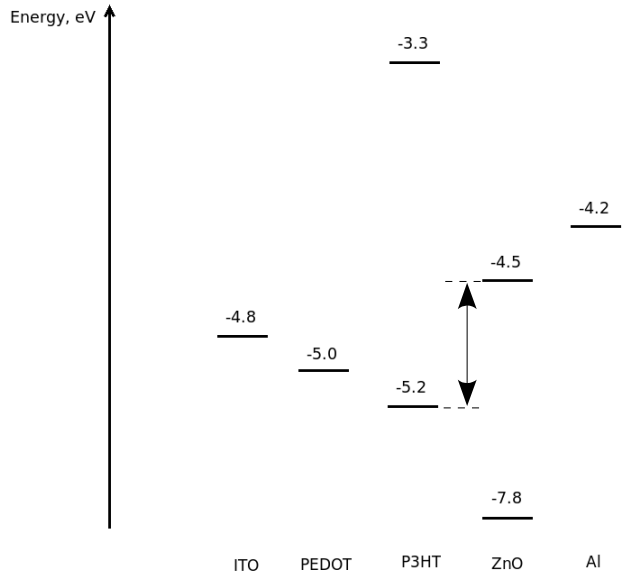

Figure 12. Energy level diagram of a ZnO-containing solar cell. The energy difference corresponding to the open-circuit voltage is shown.

The benefit of using particles of different morphologies (nanoparticle / nanorod / nanowire / nanobelt) arises from the low-dimensional nature of these nanostructures and the related size-effects ([39]–[42]). This includes improvements brought about to the bulk heterojunction architecture, namely the ZnO/polymer interface area and the presence of percolation for electron transfer in the ZnO nanostructures. If this kind of percolation is established, the excitons formed in

the semiconducting conjugated polymer can efficiently dissociate at the polymer/ZnO interface without recombination, followed by fast transfer of the formed electrons through ZnO. In addition, the nanoparticles can cause the scattering of the photons, that leads to improved photon absorption [43].

High absorption coefficients in polymeric absorbers assure that low thickness of the active layer is enough for efficient absorption. In principle, the higher the thickness of the absorbing layer, the bigger should be the efficiency of the cell. However, this is strongly limited by the low value of the exciton diffusion length in the polymeric material ($\leq$ 10 nm [41]).

In the case of ZnO, this value is higher, but the exciton generation process is not that efficient as ZnO can cover only a small portion of the solar spectrum in the UV and near-UV visible region (the band gap of ZnO is about 3.3 eV) [5]. So ZnO can be applied in hybrid solar cells preferably as electron-accepting component for increasing of conductivity of charge carriers generated by the other components of the cell.

An introductory comparative study of different morphologies of ZnO applied for P3HT-based solar cells performed at our university showed that the use of ZnO nanoparticles brings about superior cell efficiencies than nanorods and nanowires, though the efficiencies are very low [9].

In another work, an efficiency of 0.9% was reported for a cell with an active layer containing P3HT and ZnO nanoparticles [44]. However, in this case ZnO nanoparticles have been synthesised using a different synthetic procedure.

2.6. Dye-sensitization of CNT-containing and ZnO-containing solar cells

Dye-sensitization is a popular approach in the design of electrochemical solar cells. However, organic dyes can be used for the modification of excitonic hybrid solar cells as well.

In case that the solar cell incorporates CNT or ZnO, the following ways of modification have been reported:

- surface modification of ZnO. The chemical attachment of organic dyes to the surface of ZnO may lead to the formation of very efficient conjugation and hence rapid electron transfer between the dye and ZnO, as well as improved electron transfer from the semiconducting polymer to the dye can be expected [45].
  As a result of the good electron transfer from the dye to ZnO, electrons formed due to light absorption of the dye may also contribute to the solar cell current. Hence, this is the way to overcome the disadvantage of the very high band gap of ZnO by designing the dye or combination of dyes, the absorption spectra of which cover bigger part of the solar spectrum.

- surface modification of CNT. Most of the approaches involving attachment of organic dyes to CNT aim at increasing the efficiency of electron transfer from the semiconducting polymer to the CNT [46], or from the inorganic constituent to the CNT [30]. In this case, either chemical bonding (e.g., oxidation of CNT with further attachment of organic molecules) may be applied [46] or electron transfer can be achieved through van der Waals bonding [30] (figure 13). However, oxidizing of CNT decreases their conductivity because of the appearance of surface defects.

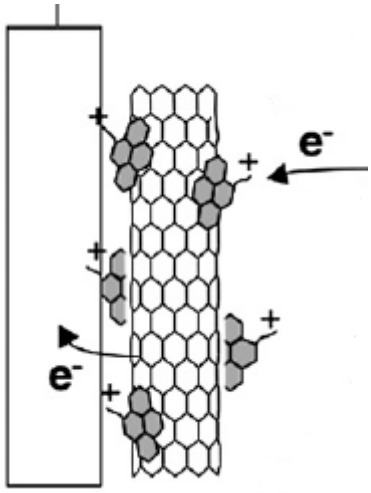

Figure 13. Mechanism of electron transfer enhancement through van der Waals bonding [30].

Summing up, the choice of the dye is determined by the following factors: (i) the presence of specific functional groups for the dye to successfully modify the surfaces of particles; (ii) its ability to provide efficient electron transfer pathways, as discussed above; and (iii) sufficient absorption coefficient and spectral coverage.

In addition, dye sensitization also promotes improved dispersion quality of the nanoparticles in the polymeric matrix, that is an important factor for the morphology of the active layer.

Various dyes have been used for the sensitization of excitonic cells, examples include: pyrene-type ([30], [9]) (max. IPCE of 9.3%), phtalocyanine-type [30] (max. IPCE of 13%), perylene-type ([45], [47]) (max. cell efficiency of 2.64%), thiophene [46] (max. cell efficiency of 1.78%).

3. EXPERIMENTAL

3.1. MATERIALS AND EQUIPMENT

Materials used:

ITO-coated glass with the surface resistivity of 20-30 Ohm/cm^2 was used as the basic substrate. Chemicals: PEDOT:PSS (1.3% aqueous solution, Sigma-Aldrich); Poly(3-hexylthiophene) (P3HT), regioregular (Sigma-Aldrich); MWCNT (Nanocyl); Acetone (Fluka); Ethanol (Panreac); Zinc acetate (Sigma-Aldrich); tetramethyl ammonium hydroxide (Sigma-Aldrich); Dimethyl sulphoxide (SDS); ethyl acetate (Panreac); toluene (Panreac); hydrazine hydrate (Sigma-aldrich); chlorobenzene (Panreac); pyrene-1-carboxylic acid (Sigma-Aldrich); acetylene, hydrogen, argon (all – Praxair) were used as purchased unless otherwise specified.

Equipment used:

Spin-coater SPS SPIN 150-V3, ultrasonic cleaner VWR, centrifuge Hettich Rotofix 32A; evaporation deposition chamber; PVD chamber; CVD chamber; micropipettes VWR; glovebag (home-constructed); DLS equipment Marvel ZetaSizer Nano; FT-Raman spectrometer Bruker RFS/100S; FT-IR spectrometer Bruker tensor 27; UV-Vis-NIR spectrophotometer Shimadzu UV-3600; UV/Vis spectrometer GBC Sintra 303; Photoluminescence spectrometer Hamamatsu C9920-02 (with copper holder); SEM/STEM Hitachi SU-70; SEM Hitachi S-4100; solar cell efficiency measurement equipment based on Keithley 228A voltage/current source, Keithley 2000 multimeter, Delta electronika power supply ES 030-10 and Philips L3 lamp.

3.2. PROCEDURES

Synthesis of zinc oxide nanoparticles

Zinc oxide nanoparticles were prepared according to the procedure used before [9], i.e., a modified procedure of the one already reported in the literature [48]. 15 ml of tetramethyl ammonium hydroxide (0.552 M) was added dropwise from a separatory funnel to 45 ml solution of zinc acetate in dimethyl sulfoxide (DMSO) (0.101 M) in a beaker under constant stirring at room temperature. Ethyl acetate was added to the mixture and a turbid solution was obtained. The turbid solution was allowed to stand for one day, and the nanoparticles were precipitated. The supernatant solution was decanted and the precipitate was washed with ethyl acetate and redispersed in ethanol. One small part of the suspension in ethanol was used to acquire the UV-Vis absorption spectrum. The ethanol was evaporated from another portion to get a concentrated suspension of the nanoparticles for the preparation of a suspension of the photoactive layer of the photovoltaic device. Besides, the solvent was evaporated from a portion of the ZnO NP suspension in ethanol and the obtained powder was subsequently used for the acquisition of Raman and photoluminescence spectra.

Surface modification of zinc oxide nanoparticles

Surface modification of zinc oxide nanoparticles with pyrene-1-carboxylic acid was done according to the procedure used before ([9], [49]). A portion of the precipitated zinc oxide nanoparticles (after the addition of ethyl acetate) was redispersed in a solution of pyrene-1-carboxylic acid in DMSO, stirred for one hour and allowed to stand for three hours. This suspension was centrifuged and the supernatant was removed and a fresh solution of PCA in DMSO was again added to the precipitate, stirred for an hour and allowed to stand overnight. This was repeated three times.

The solvent was evaporated from a portion of the functionalized ZnO NP suspension in DMSO and the brownish powder was subsequently used for the acquisition of IR and photoluminescence spectra. Attempts to record a Raman spectrum of this sample were not successful as its absorption appeared to be too high for this purposes, and the dilution procedure was more complicated from practical viewpoint than the acquisition of the IR spectrum.

Preparation of suspensions for active layer deposition

The suspensions for the deposition of the active layers of the solar cells were prepared in the following way.

A portion of the dispersion of unmodified ZnO NP in ethanol was taken, and the solvent was evaporated until a very concentrated suspension of ZnO NP was obtained. A portion of this suspension was weighed in a sample vial and then all the solvent was evaporated until a powder of ZnO NP was obtained. This was done in order to determine the concentration of ZnO NP in the concentrated suspension. After that, another portion of the suspension containing about 15 mg of ZnO NP was taken and redispersed in 5 ml of chloroform.

1 ml of the ZnO NP suspension in chloroform was added to a 4 ml sample vial with previously weighed 10 mg of P3HT. This resulted in a suspension of ZnO NP in 1% P3HT solution in chloroform, with the ZnO:P3HT mass ratio of about 3:10.

Suspensions of surface-modified ZnO NP were prepared in the following way: the suspension of PCA-modified ZnO in DMSO was centrifuged, the supernatant solution was decanted and a portion (20 mg) of the precipitate was redispersed in 5 ml of chlorobenzene. 10 mg of P3HT was weighed in a 4 ml sample vial, and then dissolved in 1 ml of the above mentioned suspension. As a result, the mass proportion of functionalized ZnO NP to P3HT was about 4:10.

The suspensions containing 0.1 mg (1% mass with respect to P3HT) of pristine multi-walled carbon nanotubes (MWCNT) were prepared for the both of the above mentioned suspensions.

All the weighing procedures (for both P3HT and MWCNT) were carried out using face protection means, i.e., goggles and a mask.

The PEDOT:PSS aqueous solution (1.3%) was used as purchased. 0.1 mg of MWCNT was added to a portion (1 ml) of the PEDOT:PSS solution (i.e., 1% mass of MWCNT with respect to the weight of the polymer) in order to check the effect of MWCNT on the conductivity and the performance of the electron-blocking layer in a solar cell.

All the suspensions containing MWCNT and ZnO were sonicated in an ultrasonic bath in order to improve the dispersion of the nanoparticles in the suspension, i.e., to disperse the agglomerates that are normally present in the pristine MWCNT powder and may be present in the ZnO colloidal solution.

In addition to the ZnO-containing suspensions, a 1% solution of P3HT in chlorobenzene was pepared by dissolving 10 mg of P3HT in 1 ml of chlorobenzene.

At first, all the P3HT-based solutions for active layer deposition were prepared using P3HT which was purchased over one year ago and stored in a vial under ambient conditions, but afterwards a dedoping procedure was performed following a method similar to the one described in the literature [44]. Briefly, 150 mg of P3HT were dissolved in 10 ml of toluene, and 2 ml of hydrazine hydrate was added. The system was heated at 60°C at constant stirring for 24 hours, after that excess of methanol was added and dark blueish precipitate was formed. The precipitate was filtered and dried on a hot plate. The procedures were done in a glovebag under nitrogen atmosphere. The dried polymer was transferred into a sample vial and closed before taking it out of the nitrogen atmosphere.

Afterwards, all the weighing steps were performed according to the following procedure: a clean sample vial was taken, closed with a cap and weighed. Then some amount of P3HT was transferred into this vial in the glovebag. The vial was closed, taken out the glovebag and weighed. This may be repeated until the desired (approximate) amount of polymer was transferred into the vial. After that, the calculated amount of solvent is added into the vial, and the polymer is dissolved. Then the other components are added. All the steps were performed inside the glovebag.

Three suspensions using distinct P3HT to ZnO@PCA ratios of 10:3, 1:2.5 and 1:5 were prepared for the dedoped P3HT sample.

Solar cell production procedure

In brief, the commercial ITO-coated glass was divided into small pieces of about 1x1 cm. Each of the pieces was labelled with a number by a scratch on the glass side. Afterwards, the glasses were submitted to a two-step cleaning in an ultrasonic bath, namely in ethanol and in acetone, followed by drying with dry air flow. Subsequently, the cleaned substrates were stored in a sealed-off vessel. Afterwards, an electron-blocking layer of PEDOT:PSS (1.3% mass aqueous solution) was deposited by spin-coating for 30 s at 2000 rpm. The use of this spin-coating parameters resulted in a film thickness of about 110 nm.

According to one of the methods used, after the spin-coating, the sample was transferred into a home-made glassy vessel with two holes in the cover, and a slow nitrogen flow was let into one of

the holes through a needle from a balloon filled with nitrogen. The other hole was left open. After some time, when the vessel was filled with nitrogen, it was transferred onto a hot plate with the temperature of about 110°C. The sample was heated for 5 min in order to evaporate the water. The heating was performed under the inert nitrogen atmosphere to avoid the possible thermooxidation of the surface of PEDOT:PSS under ambient atmosphere.

For another set of experiments, a semi-sealed-off glovebag was constructed, and all the deposition and annealing processes were performed inside of this glovebag under inert nitrogen environment. The glovebag consists of a metallic parallelepipedic frame sealed off by a thick layer of transparent polymeric film by sewing, with two gloves with long sleeves, holes for electrical wiring, pump outlet and nitrogen inlet, and a zipper along the left-hand side of the bag (see the photograph on figure 45 in the annex, p. 61). Though the glovebag is not fully isolated from the outer environment, it can assure the inert atmosphere inside of it by the creation of permanent elevated pressure inside of the bag, and hence permanent gas flow from the inside to the outside of the bag through the small holes. Before performing the spin-coating and annealing steps, all the required materials and tools were inserted into the glovebag, then the zipper was closed and nitrogen flow was let in, followed by a waiting time of 10 minutes in order to fill the box with nitrogen.
In the glovebag, the annealing was done on a home-constructed heating plate incorporating a heating element from a plastic soldering tool, a 5x5 cm aluminium plate and a shielding cover out of foamy polystyrene covered with aluminium foil (see the photograph on figure 46 in the annex, p. 61). The shielding was done in order to avoid any damage of the plastic elements of the glovebag by the high temperature of the heating plate. A normal non-shielded laboratory hot plate does not fit for this purposes as it can potentially create a threat to the plastic elements inside of the glovebag, as well as create some pressure change inside of the bag.

The various types of the active layers were deposited on top of the PEDOT:PSS layer (see the preparation procedures above), using the same spin-coating parameters (30 s at 2000 rpm). In case of pure P3HT (without addition of ZnO NP), this resulted in the active layer thickness of about 65 nm; for the films of active layers of the composition P3HT + ZnO NP and P3HT + ZnO FNP the thicknesses were 19 nm and 60 nm, respectively. And the films incorporating MWCNT (P3HT + ZnO NP + MWCNT and P3HT + ZnO FNP + MWCNT) had a thickness of 14 nm and 87 nm, respectively.
Eventually, thermal evaporation of about 1 μm thick aluminium layer was done using a thermal evaporator of the Physical Department of the University of Aveiro.

In summary, the following direct solar cell architectures were prepared:

- Glass/ITO; PEDOT:PSS; P3HT; Al (the 'reference' cell);
- Glass/ITO; PEDOT:PSS + MWCNT; P3HT; Al;
- Glass/ITO; PEDOT:PSS; P3HT + MWCNT; Al;
- Glass/ITO; PEDOT:PSS; P3HT + ZnO NP; Al;
- Glass/ITO; PEDOT:PSS; P3HT + ZnO FNP; Al;
- Glass/ITO; PEDOT:PSS; P3HT + ZnO NP + MWCNT; Al;
- Glass/ITO; PEDOT:PSS; P3HT + ZnO FNP + MWCNT; Al;
- Glass/ITO; PEDOT:PSS; P3HT + ZnO FNP + MWCNT (forest); Al.

Another set of samples was prepared by direct deposition of the active layer suspensions onto the cleaned ITO-coated glass. These samples were used for the acquisition of the photoluminescence and UV-Vis absorption spectra.

Attempts to prepare inverted cell structures, i.e., depositing the electron-blocking PEDOT:PSS layer on top of the active layer, were unsuccessful for the samples with low concentration of ZnO NP because of high hydrophobicity of the P3HT-based layer which prevented wetting by the aqueous PEDOT:PSS solution which is necessary for the spin-coating of the film.

CVD growth of carbon nanotubes on ITO substrate

The chemical vapour deposition (CVD) growth of carbon nanotubes was performed using acetylene as carbon source in an argon - hydrogen atmosphere and the substrate of ITO-coated glass on which a thin layer of iron (1 nm) had been deposited by physical vapour deposition (PVD). Two different temperatures were used for the CVD growth, namely 500 and 750°C.

At first, the substrate was loaded into the chamber, and a pre-heating step was done for 5 min in argon atmosphere (1000 standard cubic centimetres per minute (sccm)). After that, another pre-heating step at 200 sccm argon flow and 500 sccm hydrogen flow was performed for 2 min. Finally, the deposition was carried out at 10 sccm acetylene flow, 100 sccm hydrogen flow and 400 sccm argon flow for 10 min.

Transfer of MWCNT forest

In order to check the possibility of the MWCNT forest transfer, the following procedure was used. An ITO-coated glass substrate with a P3HT layer deposited on top of it by spin-coating (2000 rpm, 30 s) was taken and put onto a hot plate. The aligned MWCNT forest deposited on a silicon substrate (kindly supplied by Mr. Diogo Mata) was then put on top of the P3HT film with the nanotubes touching the polymeric film. Afterwards, several pieces of glass were put on top of the silicon substrate to create some pressure. Then the substrate was heated up to 170°C, the temperature was kept for 5 minutes, and the sample was removed from the hot plate and allowed to cool down. Finally, the silicon substrate was removed, leaving the nanotube forest attached to the P3HT substrate.

A second MWCNT forest transfer process was carried out. A direct solar cell structure was created by deposition of PEDOT:PSS layer via spin-coating, annealing of the layer, followed by the deposition of a thick active layer (P3HT + ZnO FNP) via evaporation of the solvent after covering the sample with several drops (0.04 ml) of active layer solution. This was done to obtain a thick film (at least a micrometre thick) of the active layer, whereas the usual spin-coating procedure would require a big number of deposition steps for getting the same thickness value. After this, the MWCNT forest was transferred from the silicon substrate by a procedure similar to the one described above, but without any pressure on top of the substrate (because of the spacial limitations caused by the operation inside of the glovebag). After the transfer, an aluminium layer was deposited via thermal evaporation deposition on top of the active layer containing the transferred MWCNT forest.

Characterization of the materials

The particle size and zeta-potential of ZnO NP was determined using a Marvel ZetaSizer Nano measurement device and diluted suspension of ZnO NP in ethanol. A similar measurement was performed for the ZnO FNP, however, the FNP appeared to be agglomerated in common solvents, hence, unrealistic data have been obtained as a result of these measurements.

As it was mentioned above, FT-Raman spectrum of the ZnO NP powder was acquired (using FT-Raman spectrometer Bruker RFS/100S, 500 scans with the laser energy of 250 mW), and FT-IR spectrum of the functionalized ZnO NP powder was acquired using Bruker tensor 27 FT-IR spectrometer.

Light absorption of the active layers was analysed using a Shimadzu UV-3600 UV-Vis-NIR spectrophotometer.
The photoluminescence spectra of the above mentioned powders and films of active layers on ITO-coated glass were obtained using a Hamamatsu C9920-02 photoluminescence spectrometer.

The microstructure of the active layers, CVD-grown carbon nanotubes and the transferred MWCNT forests was analysed by scanning electron microscopy (SEM) using two microscopes: Hitachi SU-70 and Hitachi S-4100 (SEM/STEM). The samples did not require any preliminary preparation steps before the SEM observations, as they possess an enough level of conductivity.
The latter microscope was also used for the analysis of the ZnO NP and ZnO FNP. The preparation procedure for the samples for this kind of analysis involved immersion of the TEM grids into the dispersion of ZnO NP in ethanol and into the dispersion of ZnO FNP agglomerates in acetone, respectively.

Solar cell efficiency measurements

All the cells produced during the work were checked for the presence of photovoltaic effect by measuring their current-voltage characteristics using the current-voltage measurement equipment and a solar illumination simulating lamp with controllable illumination intensity. In all measurements, the light intensity was set to 1000 W/m^2.
Before the measurements, the ~1x1 cm cell was scratched with a needle in order to obtain 4 separated square sections, and the deposited layers at one of the edges were removed, after that silver paste was painted onto that part of the ITO, on the adjacent glass edge and on the area of glass of the same size on the opposite side of the sample (see figure 14). Then the silver paste was allowed to dry. The silver paste deposition was done in order to assure the contact between the ITO and the tip of the electrode of the measuring device, as the ITO layer is put in contact with the corresponding electrode from the top-side, whereas a contact between the aluminium layer and another electrode is established through the copper plate located beneath the sample.

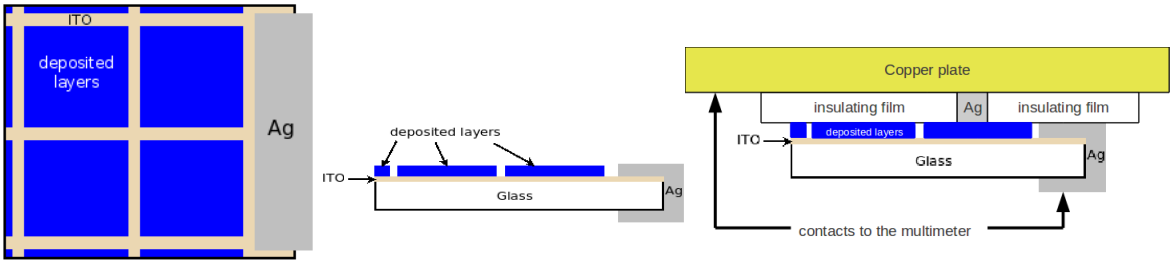

Figure 14. Sketch of the contacts of a solar cell: top-view (left); side-view (centre); side-view with copper holder (right).

4. Results and discussion

In this chapter, the characterisation of the materials prepared is first discussed, including the characterisation of ZnO NP and dye-modified ZnO NP by DLS and zeta-potential, SEM, FT-IR and UV-Vis spectroscopy (4.1.). The study of the morphology of the various active layers and their constituents by SEM is discussed in (4.2.). The optical properties of the active layers are studied by means of UV-Vis-NIR spectroscopy in (4.3.), and by photoluminescence spectroscopy in (4.4.). Finally, in 4.5. the results of the measurement of current-voltage curves of the various solar cells are presented and discussed.

4.1. Characterisation of the ZnO NP

According to the Dynamic Light Scattering experiment using the ZetaSizer Nano equipment, the synthesised ZnO NP have an average particle size of about 12 nm. The SEM observations give a similar result of about 5-15 nm (see figure 15).

The zeta-potential measurement of ZnO NP/ethanol suspension resulted in a value of – 18 mV, which corresponds to a moderately stable suspension.

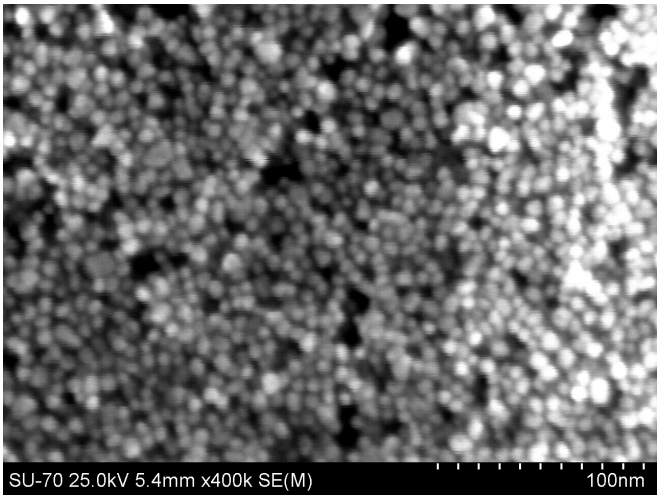

Figure 15. SEM image (25 kV) of ZnO nanoparticles.

The functionalised ZnO NP, as it was already mentioned in the experimental part, appear to be agglomerated in all of the solvents that were used, hence variable and non-realistic values of several hundreds of nanometres were determined by this method. The SEM observations show that the size of the particles is about 5-10 nm (figure 16).

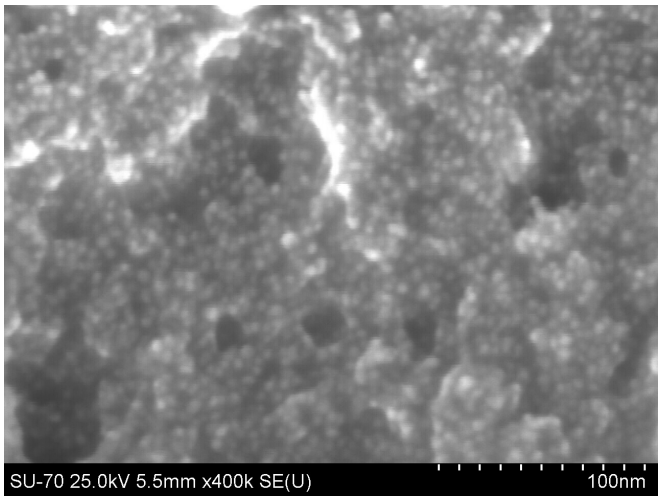

Figure 16. SEM image (25 kV) of PCA-modified ZnO nanoparticles.

The zeta-potential of the PCA-modified ZnO NP/ethanol suspension was + 20 mV, which corresponds to a moderately stable suspension. However, this value is quite unreliable because the particles did aggregate.

As a result, it can be said that the modification of ZnO NP with pyrene-1-carboxylic acid (PCA) does not significantly alter the particle size of the NP, though it changes the chemical structure and charge of their surface.

This conclusion can be further confirmed by the analysis of the Raman and IR-spectra of the unmodified and PCA-modified ZnO NP, correspondingly.

The Raman spectrum of the unmodified ZnO NP is represented on figure 17. From this spectrum it is possible to conclude that the surface of the NP is covered with acetate anions, namely the bands at 3033 and 2987 cm^{-1} (as well as the band on the left shoulder of the latter one) correspond to the asymmetrical stretching of C-H bonds in CH_3 group of the acetate anion, the most intense band at 2929 cm^{-1} corresponds to the symmetrical stretching of the same bonds [50]. The bands caused by deformational vibrations of the CH_3 group can be found at 1452 and 1345 cm^{-1} [51]. Finally, among the characteristic bands asymmetrical stretching of conjugated double bond of carbonyl group in COO^- anion can be detected at 1590 cm^{-1}. Due to the high delocalization caused by the presence of charge and, presumably, bridge-type coordination to Zn atoms [52], this band appears to be much shifted compared to the normal position of carbonyl absorption. The symmetric stretching of these bonds gives rise to the band at 1419 cm^{-1}. The broad band at 3200-3400 cm^{-1} is most likely caused by the absorption of water, as ZnO NP are very hygroscopic.

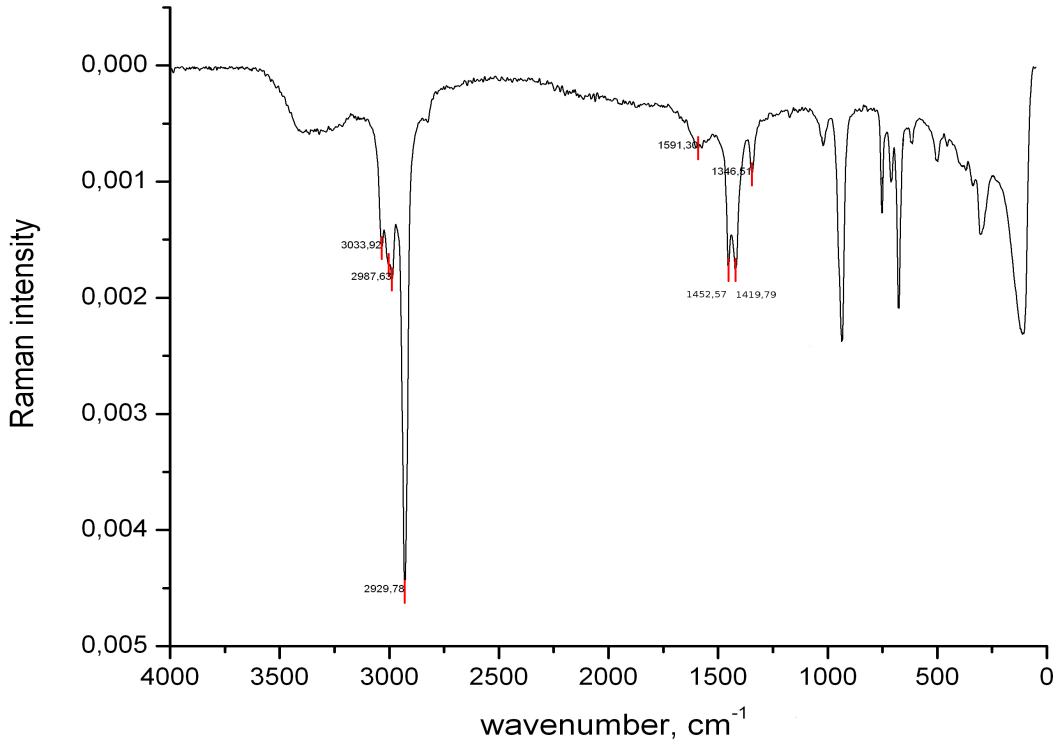

Figure 17. FT-Raman spectrum of zinc oxide nanoparticles.

At the same time, it is impossible to find the characteristic bands for ZnO vibrations (at 437 and 408 cm^{-1} [50]), probably because of the relative weakness of these signals and high baseline level in the low-energy spectral region.

If we compare this spectrum to the one obtained in the previous work following the same synthesis method [9], it can be seen that in our case there is no evidence of the absorption of ethyl acetate ($CH_3COOC_2H_5$) on the surface of ZnO NP (only acetate counter-anions (CH_3COO^-) appear to be present), though there was one in that work. One of the reasons for this could be that the ethyl acetate was desorbed from the surface during solvent evaporation from the ZnO NP suspension. At the same time, it is also probable that it was not adsorbed during the synthesis at all and just acted as a non-solvent medium for the precipitation of ZnO NP.

As regards the PCA-modified ZnO NP, its spectrum is shown in figure 18.

The following characteristic bands can be identified on this spectrum: firstly, a broad band around 3450 cm^{-1} is observed which is attributed to water as the substance is highly hygroscopic. Then,

bands below 3000 cm^{-1} are the evidence of the presence of saturated groups. Most likely, they correspond to the asymmetrical and symmetrical stretching of C-H bonds of the CH_3– group of the acetate anion. The presence of the acetate anion is further confirmed by the bands at 1591 and around 1410 cm^{-1} that correspond to asymmetrical and symmetrical stretching of the $–COO^-$ group of the acetate anion. Near to the 1591 cm^{-1} band, there is another band at 1616 cm^{-1} that corresponds to the asymmetrical stretching of the $–COO^-$ group of the pyrene-1-carboxylate anion. The band of the symmetrical stretching of this group coincides with the band for the similar stretching of the acetate anion, i.e., it is located around 1400 cm^{-1}. The band around 1550 cm^{-1} corresponds to the stretching of C=C bonds of the pyrenic aromatic system. Finally, the bands around 2350 cm^{-1} are likely to be caused by atmospheric CO_2, so they should be considered as an artefact.

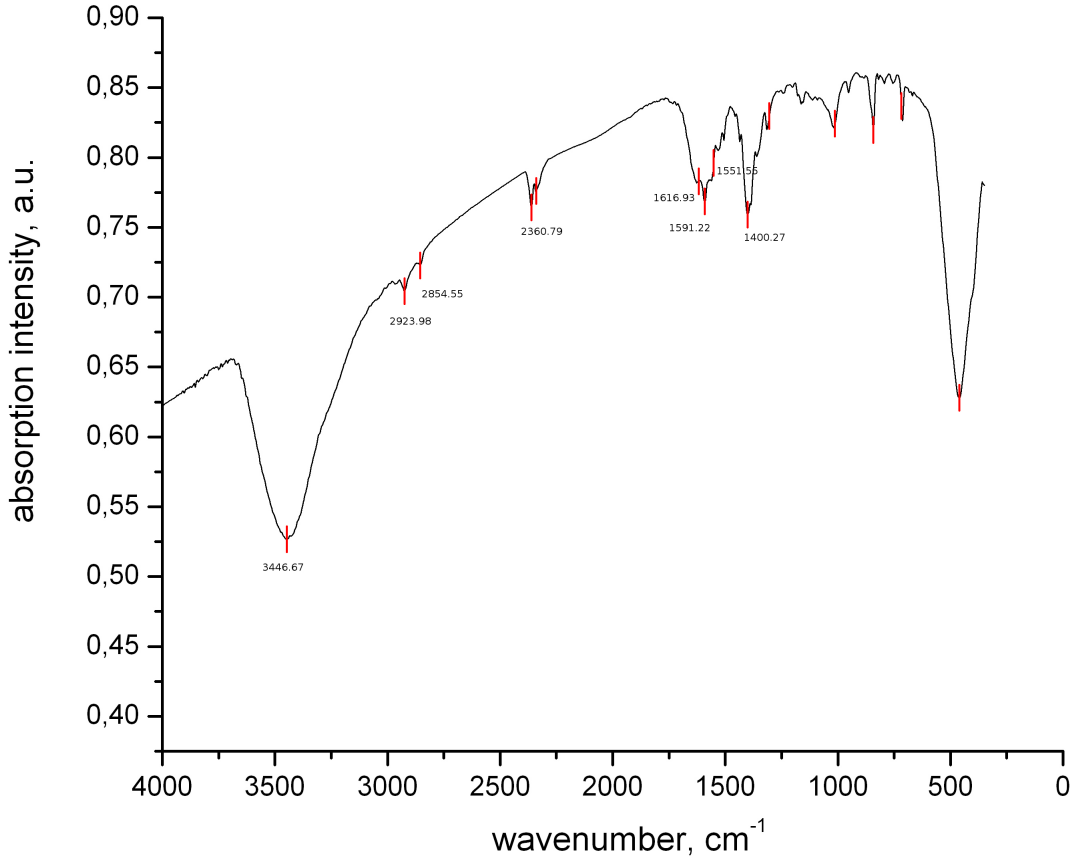

Figure 18. FT-IR spectrum of PCA-modified ZnO nanoparticles.

UV-Vis absorption spectrum of ZnO NP powder deposited on a glass substrate from the dispersion in ethanol is represented on figure 19.

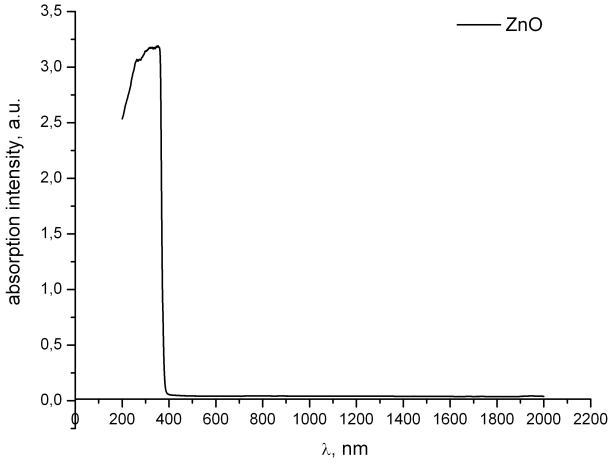

Figure 19. UV-Vis absorption spectrum of the ZnO NP powder deposited on glass.

The spectrum is a typical step-like semiconductor light absorption spectrum (maximal absorption at about 366 nm and below). The decrease in absorption below 250 nm is an artefact caused by the spectral baseline acquisition using clean glass substrate as a reference. The reason for this is that the region below 250 nm corresponds to the absorption of the glass, so such an effect is likely to have been caused by a small discrepancy in the thickness between the sample substrate and the reference one.

In order to determine the band gap value, the data of the spectrum above are used for the construction of an $(\alpha h\nu)^2$ versus $h\nu$ plot (figure 20) that is used for the determination of the band gap for direct band gap semiconductors. According to the linearisation of the fragment of the spectrum, the band gap value equals about 3.14 eV.

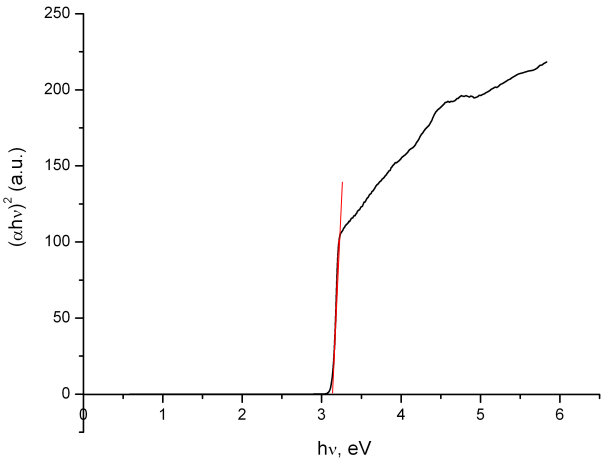

Figure 20. $(\alpha h\nu)^2$ versus $h\nu$ plot for the determination of the band gap of ZnO.

In order to determine the particle size of ZnO NP by spectroscopy, a UV-Vis absorption spectrum of the suspension of ZnO NP in ethanol was acquired (see figure 21). Again, this is a similar step-like plot. An $(\alpha h\nu)^2$ versus $h\nu$ plot (figure 22) was constructed using the data of this spectrum, and the band gap value for ZnO NP equals approximately 3.25 eV that is slightly higher than the value obtained before for the powder.

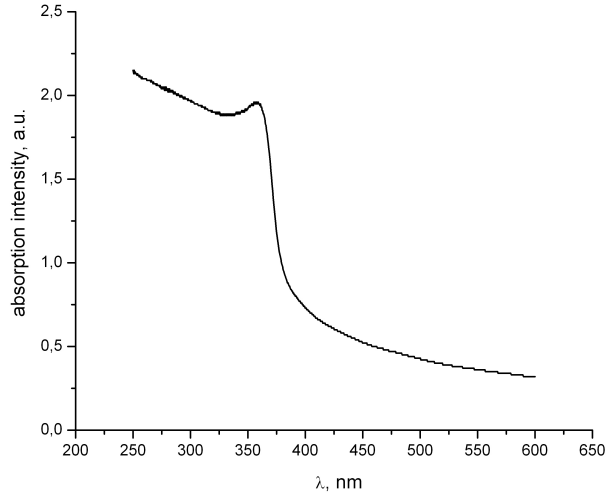

Figure 21. UV-Vis absorption spectrum of the ZnO NP suspension in ethanol.

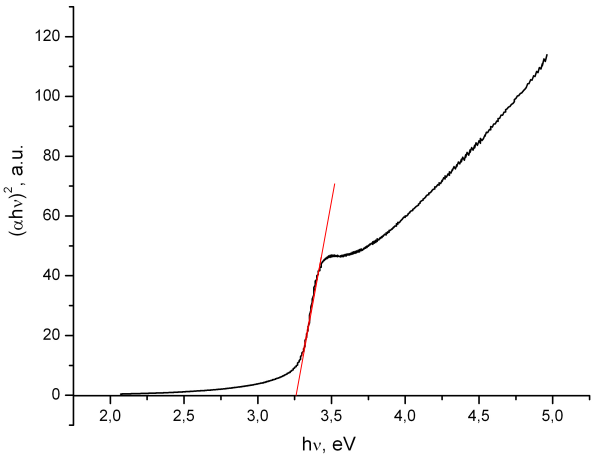

Figure 22. $(\alpha h\nu)^2$ versus $h\nu$ plot for the determination of the band gap of ZnO NP.

The particle size can be calculated out of the band gap values by solving Brus equation:

$$E_g = E_g^{bulk} + \frac{h^2}{8R^2}\left[\frac{1}{m_e^*} + \frac{1}{m_h^*}\right] - \frac{1.8e^2}{4\pi\varepsilon\varepsilon_0 R} - \frac{0.124e^4}{\hbar^2\left(4\pi\varepsilon\varepsilon_0\right)^2}\left[\frac{1}{m_e^*} + \frac{1}{m_h^*}\right]^{-1}$$

where E_g is the band gap of the ZnO NP, E_g^{bulk} is the band gap of the bulk ZnO semiconductor, h is the Planck's constant, R is the diameter of the nanoparticles, m_e* is the electron effective mass, m_h* is the hole effective mass, ε is the relative permittivity, ε_0 is the permittivity of vacuum, e is the charge of an electron. ε_0=8.85·10^{-12} m^{-3}·Kg^{-1}·s^4·A^2, e=1.6·10^{-19} C, h=6.626·10^{-34} m^2·Kg/s, $\hbar$=1.055·10^{-34} m^2·Kg/s, m_0=9.109·10^{-31} Kg, and for ZnO: ε=8.5, E_g^{bulk}=3.2 eV, m_e=0.26·m_0, m_h=0.59·m_0 [9].

The solution of this equation results in the value of 6.27 nm that is in good correlation with the SEM and DLS data.

The UV-Vis absorption spectrum of PCA-modified ZnO NP deposited on glass substrate from suspension in ethanol is shown on figure 23.

As it can be seen from the spectrum, the intense absorption band of ZnO appears in the region around and below 300 nm, and above this value another, yet not so intense band is observed. The latter one corresponds to the absorption of PCA, that can be proved via comparison with the UV-Vis absorption spectrum of pure PCA (figure 24).

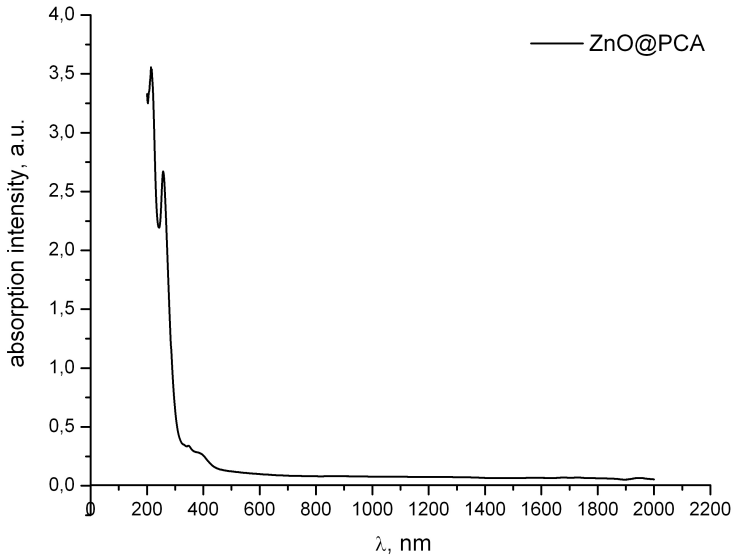

Figure 23. UV-Vis absorption spectrum of the powder of ZnO@PCA NP deposited on glass.

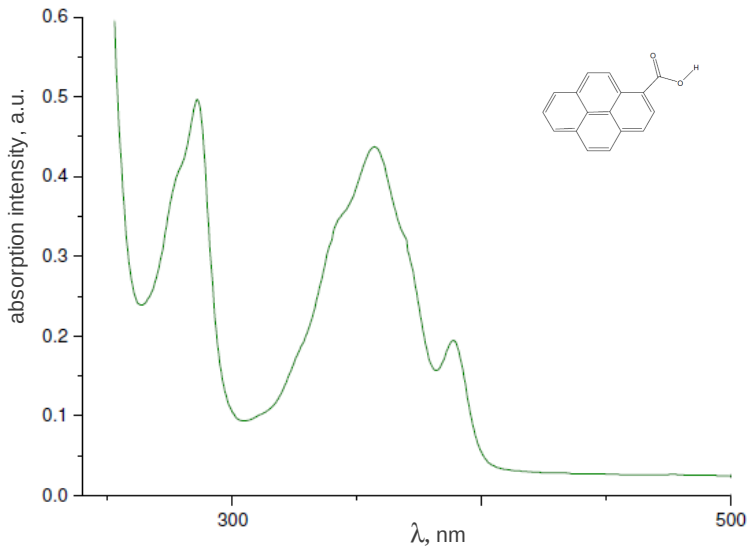

Figure 24. UV-Vis absorption spectrum and chemical structure of PCA [9].

However, unlike the PCA absorption spectrum, on the spectrum of ZnO@PCA the band extends up to about 430 nm and all the PCA bands look like a shoulder of the ZnO absorption band. That is likely to be a consequence of the relatively low concentration of the PCA chromophores when compared to ZnO.

4.2. SEM OBSERVATION OF THE MATERIALS

CVD-grown MWCNT on ITO-coated glass substrate

As it was shortly mentioned before, the main objective of growing carbon nanotubes directly on the substrate of ITO-coated glass was to obtain well-aligned 'forests' of MWCNT with small distances between the nanotube walls and direct contact between the nanotubes and the layer of the ITO transparent conductor. As a result, this design could be used for the significant improvement of the conductivity of the active layer, as well as for the realization of the 'bulk heterojunction' concept, with the nanotubes representing pathways for the charge carriers to one of the electrodes.

However, direct CVD growth did not appear to be a successful method for the preparation of the MWCNT forest. Though some of the tube-like objects grow even at the operation temperature of 500°C (see figure 25), their surface density is relatively low and uneven (compare figures 25 b,c), they are relatively short (though the length is not a problem for this particular application) and possess a lot of defects (figure 25 d).

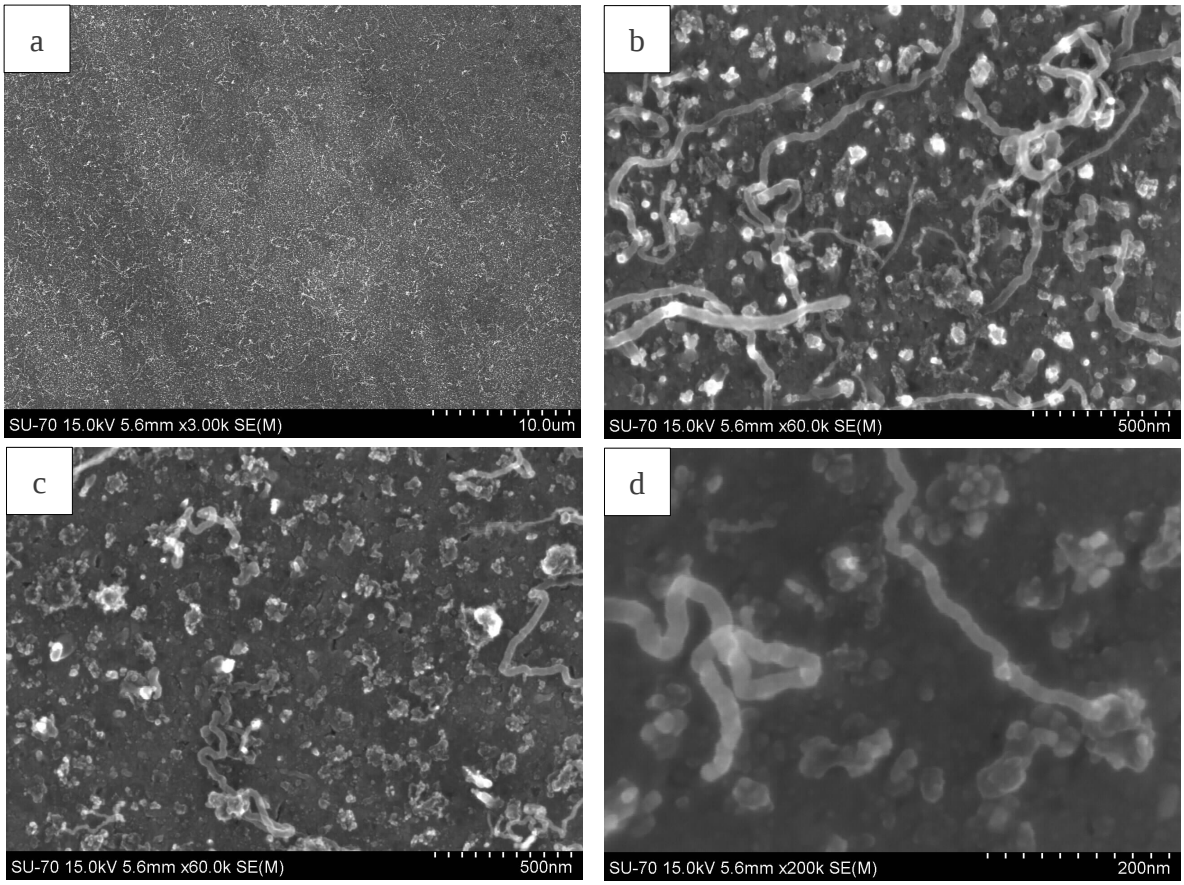

Figure 25. SEM image (15 kV) of carbon nanotubes on ITO-coated glass CVD-grown at 500°C:
a) magnification 3000 X; b,c) magnification 60000 X; d) magnification 200000 X.

The white particles that are seen on the images are the iron seeds that were used as catalyst for CNT growth. It should be also noted that there was no change to the ITO layer, and its conductivity remained practically unaltered after the CVD experiment (according to the simple checks using a multimeter).

If we consider the SEM images for the CVD experiment conducted at 750°C (figure 26), it can be seen that the nanotube growth process takes place much more intensively, however, there appear to be a lot of defects on the nanotubes, so they actually look like entangled wires (figure 26 b,c). Moreover, when comparing with the previous result, the higher temperature causes coarsening of the iron particles of the seeding layer and as a consequence, less seeding centres are available for the nanotube growth.

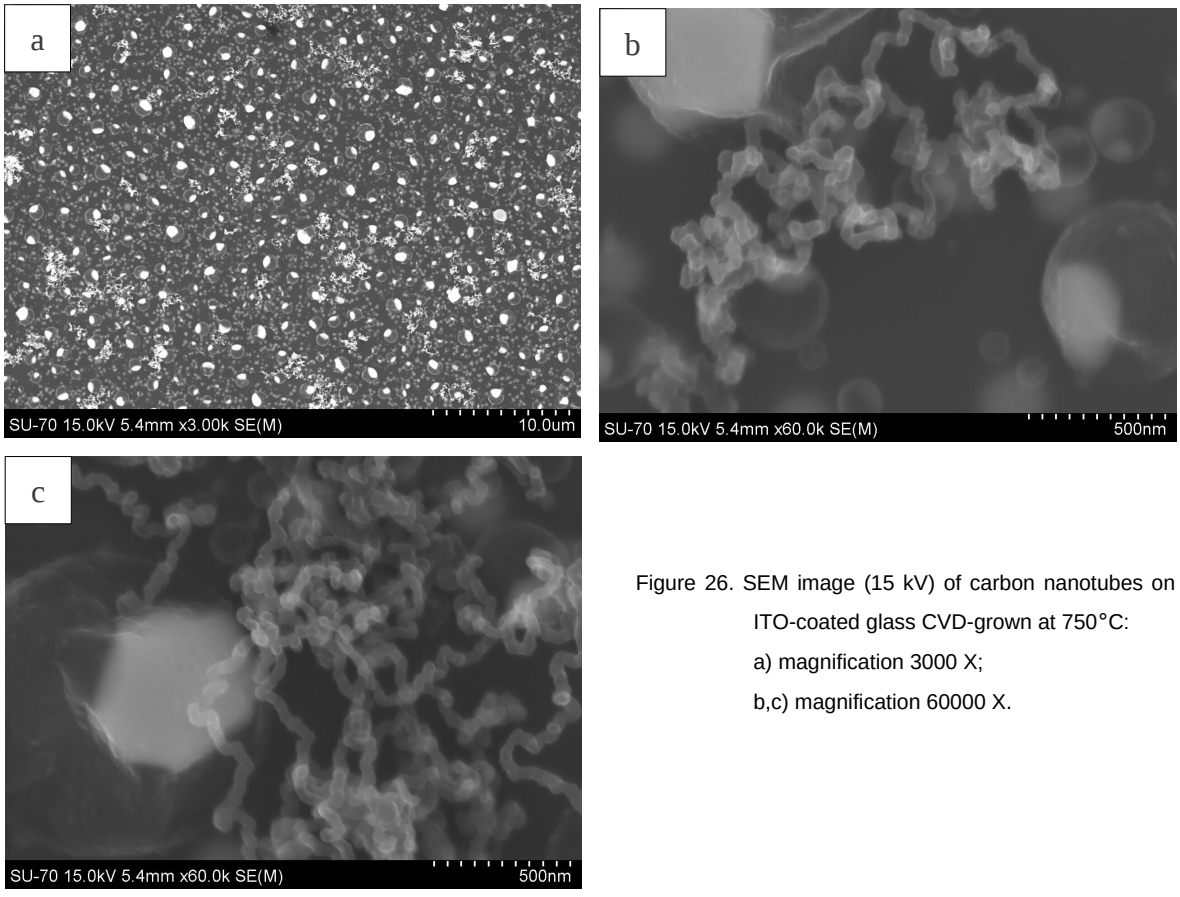

Figure 26. SEM image (15 kV) of carbon nanotubes on ITO-coated glass CVD-grown at 750°C:
a) magnification 3000 X;
b,c) magnification 60000 X.

Though the main drawback of the process at this temperature is that the ITO/glass substrate does not withstand it, and after the experiment the sample does not possess any conductivity. However, the image contrast during SEM observations of the sample is present, and as the contrast relies on a certain level of conductivity of a sample, it is also possible that the conductive ITO layer actually

decomposes into small separated sections. But for the purpose of the preparation of solar cells such a sample is of no use as it can not serve as continuous electrode.

Finally, another disadvantage is that at this high temperature thermal stresses develop in the glass, and at the contact with the heating surface softening of the glass occurs, so it appears to be glazed and cracked after taking it out of the CVD chamber.

In conclusion, the ITO-coated glass substrate that was used for the direct CVD growth did not appear to be the right one for growing the aligned forest of MWCNT. A possible solution for this problem could be using higher temperature-resistant glass, or applying plasma-assisted CVD process, but this was beyond the time frame of this work.

Transfer of the MWCNT forest

The forest of long (about 300 µm) MWCNT previously grown via CVD on silicon substrate was successfully transferred to the P3HT film on ITO-coated glass substrate (see figure 27).

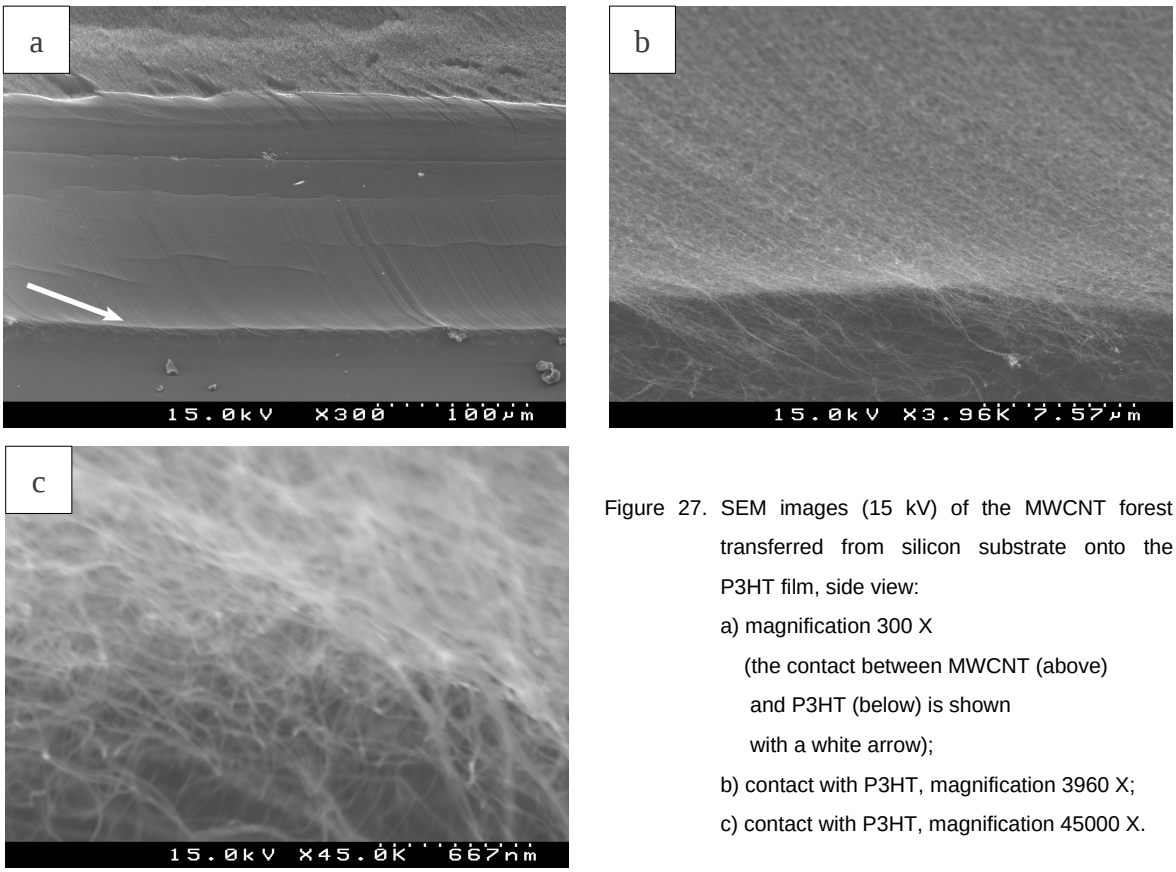

Figure 27. SEM images (15 kV) of the MWCNT forest transferred from silicon substrate onto the P3HT film, side view:
a) magnification 300 X
(the contact between MWCNT (above) and P3HT (below) is shown with a white arrow);
b) contact with P3HT, magnification 3960 X;
c) contact with P3HT, magnification 45000 X.

Most importantly, during the transfer process the alignment of the nanotubes was preserved, and there is no significant change in the dispersion quality of the nanotubes both in the upper part and in the bottom (i.e., in the part that is in contact with P3HT). Besides, no significant defects seem to be introduced to the nanotubes because of the transfer process.

An attempt was made to spin-coat another P3HT layer on top of this transferred MWCNT. After the spin-coating and annealing the MWCNT forest was still attached to the underlying P3HT layer (with some minor distortions at the edges), and it was covered with P3HT. However, due to the influence of the solvent (chlorobenzene) a significant number of defects (bendings and entanglements) is introduced to the nanotubes (see figure 28). Besides, some bundling and degradation of dispersion quality can be noticed, though this is a minor effect.

Because of the bending of the nanotubes that is likely to change their conductivity, coating of MWCNT forest with P3HT from its solution does not seem a good option.

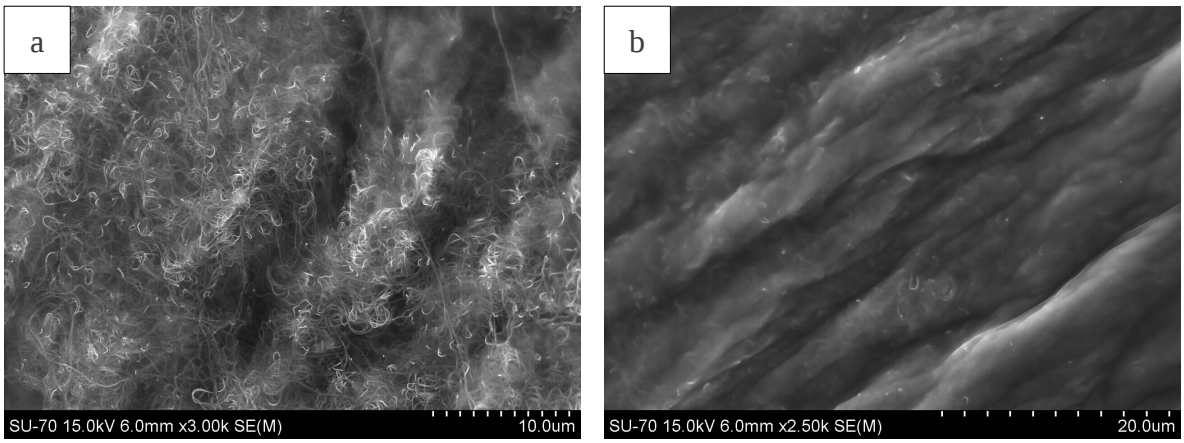

Figure 28. SEM images (15 kV) of the MWCNT forest spin-coated with P3HT:
a) magnification 3000 X; b) magnification 2500 X.

Active layers

The SEM images of the surface of spin-coated MWCNT / P3HT composite film (deposited from chlorobenzene solution) can be seen on figure 29. Due to the similar high electrical conductivity of both carbon nanotubes and P3HT it was impossible to obtain the contrast on SEM images between the polymeric part and the nanotubes (or their agglomerates, it remains unclear). However, some particle-like objects can be seen, which are thought to be agglomerates of carbon nanotubes with adsorbed P3HT.

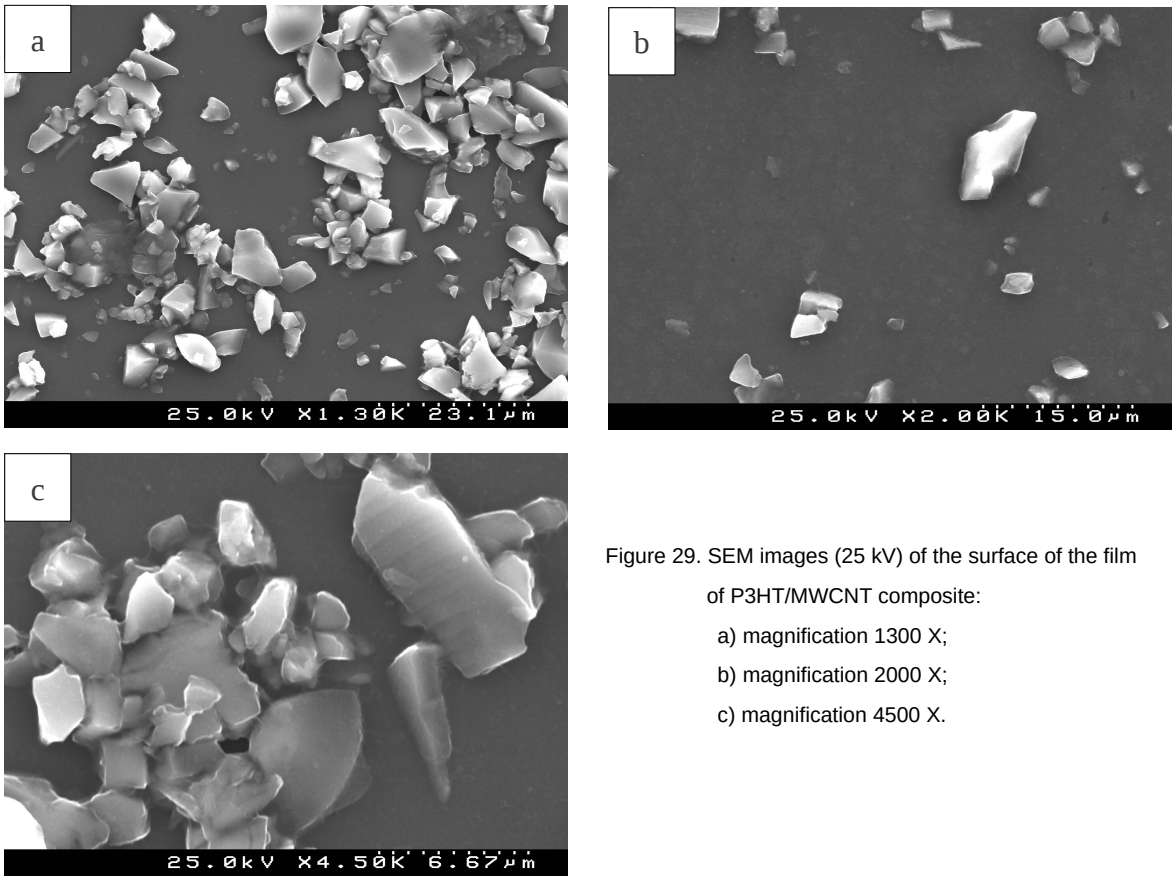

Figure 29. SEM images (25 kV) of the surface of the film of P3HT/MWCNT composite:
a) magnification 1300 X;
b) magnification 2000 X;
c) magnification 4500 X.

The SEM images of the P3HT / ZnO composite film are shown on figure 30. It can be seen that the ZnO nanoparticles appear to be strongly agglomerated with the agglomerate size of about 0.5-1 µm, and the agglomerates are not interconnected. According to the images, the size of the NP varies in the range of 10-40 nm.

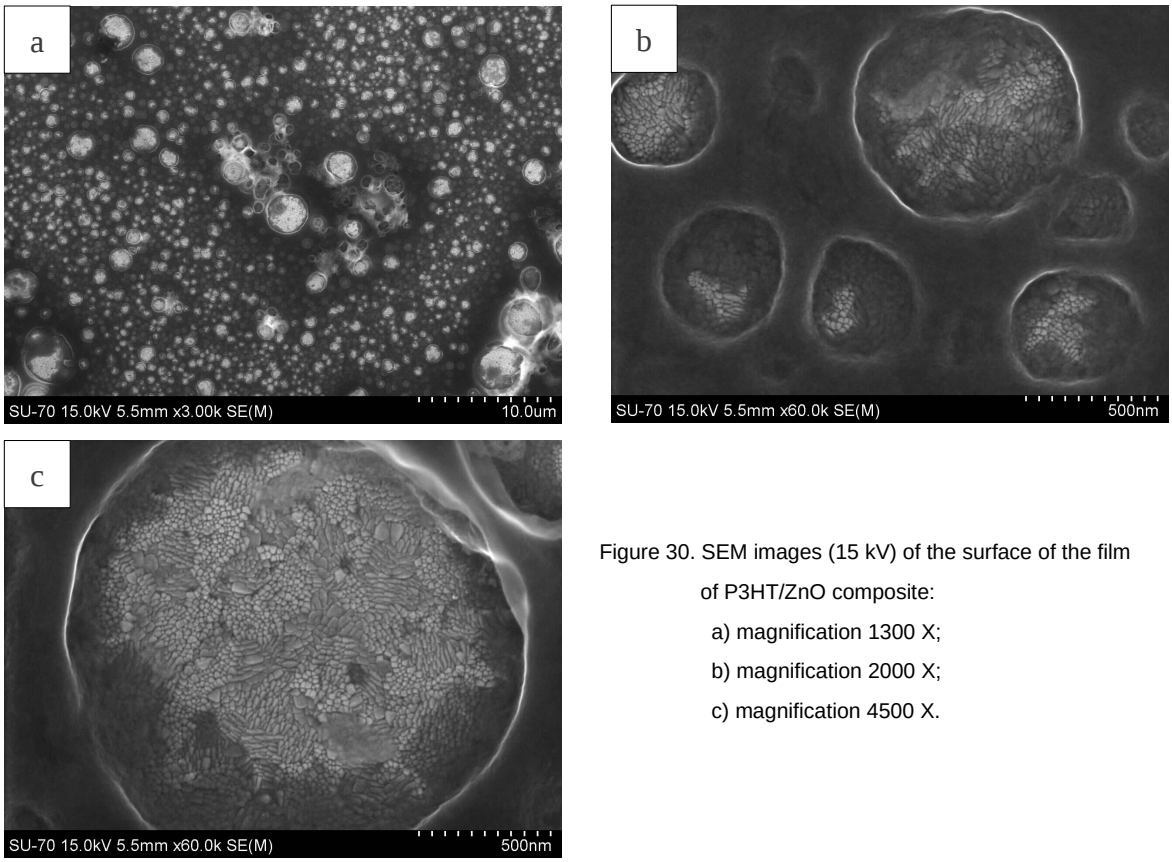

Figure 30. SEM images (15 kV) of the surface of the film of P3HT/ZnO composite:
a) magnification 1300 X;
b) magnification 2000 X;
c) magnification 4500 X.

A similar microstructure is obtained for the film of P3HT / PCA-modified ZnO composite (figure 31). In this case, the agglomerates are a little bit smaller, their distribution in the polymeric matrix is better than in the previous case, though the functionalisation of the surface of ZnO did not bring about good dispersion quality of the nanoparticles in the P3HT matrix.

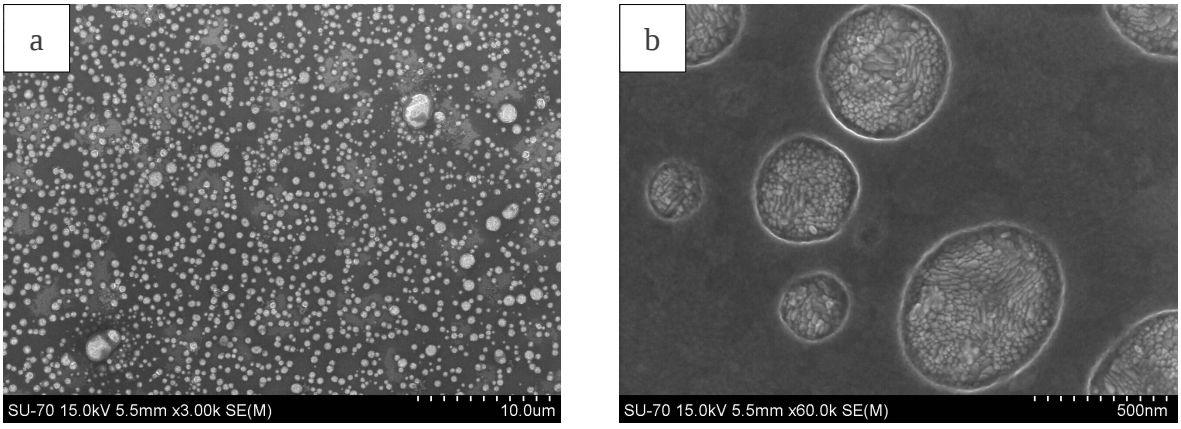

Figure 31. SEM images (15 kV) of the surface of the film of P3HT / ZnO@PCA composite:
a) magnification 3000 X; b) magnification 60000 X.

In the case of the film composition P3HT / unmodified ZnO NP / MWCNT, the morphology remains the same as the one observed for the above discussed samples (see the SEM image on figure 32). And again, as in case of P3HT / MWCNT film, there is no evidence of the presence of carbon nanotubes in the composite because of the absence of image contrast.

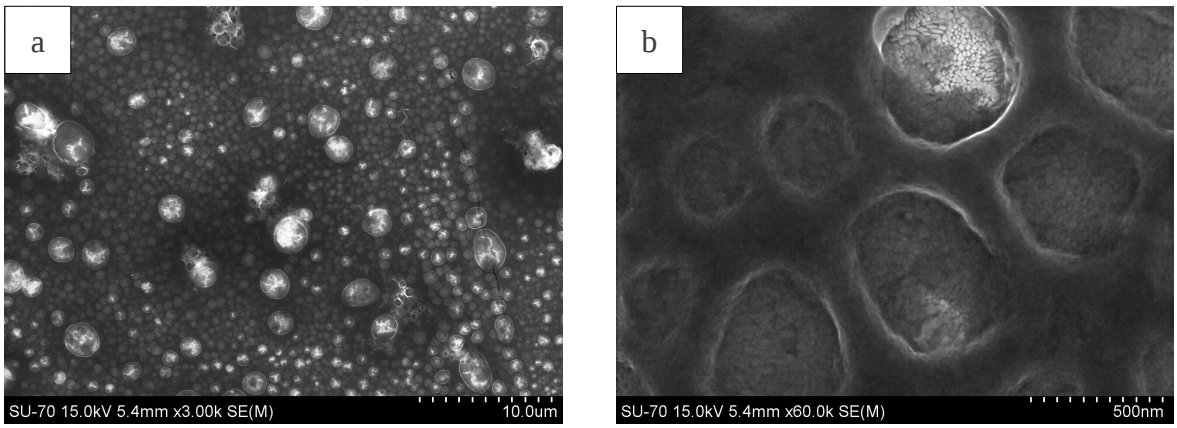

Figure 32. SEM images (15 kV) of the surface of the film of P3HT / ZnO / MWCNT composite:
a) magnification 3000 X; b) magnification 60000 X.

Finally, the SEM image of P3HT / PCA-modified ZnO NP / MWCNT composite shown on figure 33 contains various morphological features. On one hand, the dispersion quality of ZnO@PCA is mostly bad, and the particles appear to be agglomerated (figure 33a). However, in some parts of the sample the visualisation of the carbon nanotubes is possible, and it can be clearly seen that the MWCNT appear to be aggregated (figure 33a, top-left side, greyish region marked with a white arrow) so their dispersion quality is rather poor.

Another interesting phenomenon that is visualised in some areas of the sample is the interaction of MWCNT with ZnO@PCA agglomerates (figure 33 b,c). On these pictures, it can be seen that if a carbon nanotube establishes a contact with the agglomerate of ZnO@PCA, it leads to the dispersion of the agglomerate, though the agglomerates that did not form a contact like this remain unaltered. It is clear that this effect is a direct consequence of the surface modification of ZnO NP, as it was absent in the films prepared with the unmodified ZnO NP.

The mechanism of interaction that causes it is probably the same as discussed before (figure 13, p.17). As a result, the PCA may not only improve the conductivity between the ZnO nanoparticle and CNT as it was proposed, but it also serves as a surface stabilizer that improves the dispersion

quality of ZnO@PCA by attracting the nanoparticles to the surface of CNT and breaking the agglomerate that the particles tend to form.

In addition to the improvement of ZnO NP dispersion quality, such kind of interaction is likely to have been a factor that enabled the visualisation of the MWCNT via increasing the conductivity of the nanotubes which are in contact with ZnO@PCA NP.

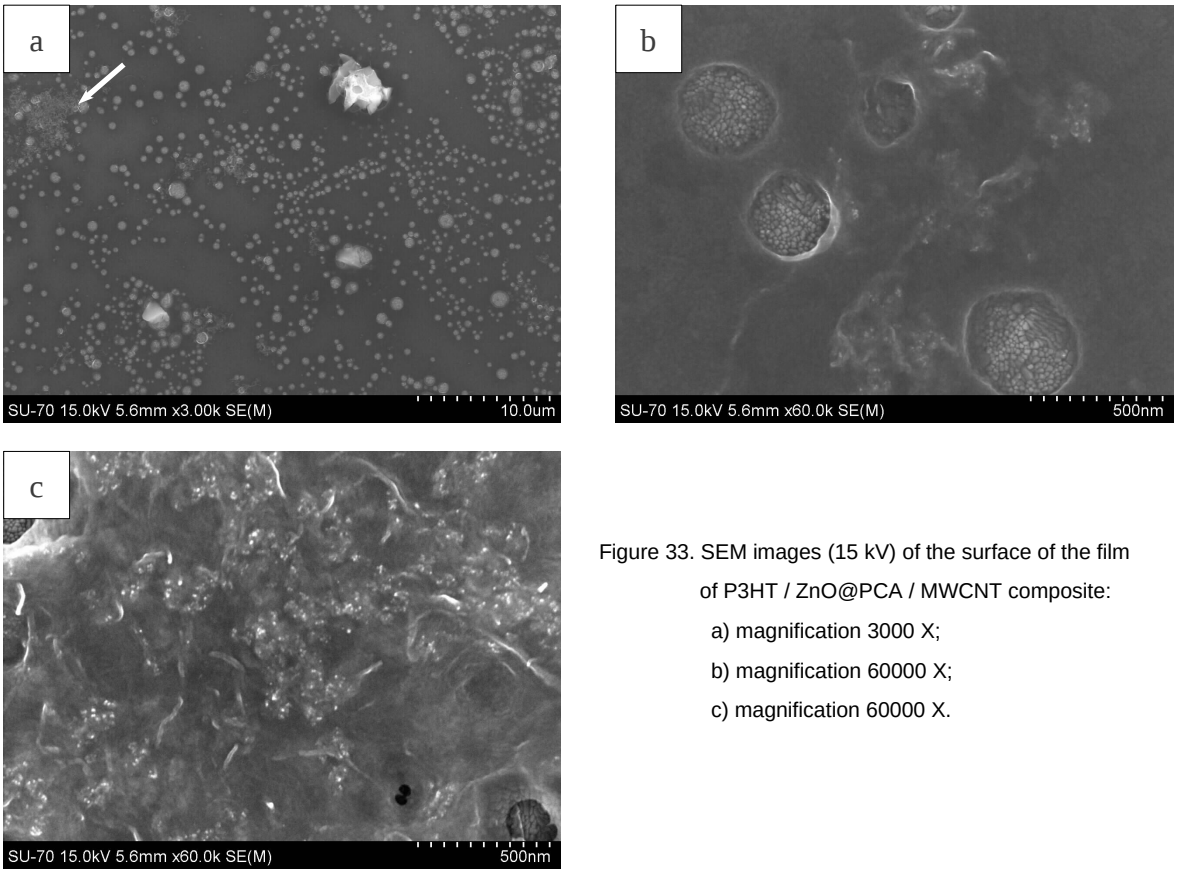

Figure 33. SEM images (15 kV) of the surface of the film of P3HT / ZnO@PCA / MWCNT composite:
a) magnification 3000 X;
b) magnification 60000 X;
c) magnification 60000 X.

However, due to the fact that the distribution quality of the nanotubes is pretty bad, the positive effect of CNT on dispersion quality of ZnO@PCA NP occurs only in limited areas of the sample. In order to overcome this, the transfer of MWCNT forest was performed onto the solar cell made of the films of PEDOT:PSS and the P3HT + ZnO@PCA (10:3) active layer, according to the transfer process used before (see p.25 for details). Finally, an Al layer was deposited on top of the forest.

4.3. UV-Vis-NIR SPECTROSCOPY OF THE ACTIVE LAYERS

In order to compare the effect of various components of the active layers of the solar cell on the spectral coverage and light absorption intensity, the ultraviolet-visible-near-infrared (UV-Vis-NIR) absorption spectra of the samples of various active layers spin-coated onto the ITO-coated glass were measured. The spectra are represented on figure 34, the corresponding active layers are the following: a) P3HT + ZnO; b) P3HT + ZnO@PCA; c) P3HT + ZnO + CNT; d) P3HT + ZnO@PCA + CNT.

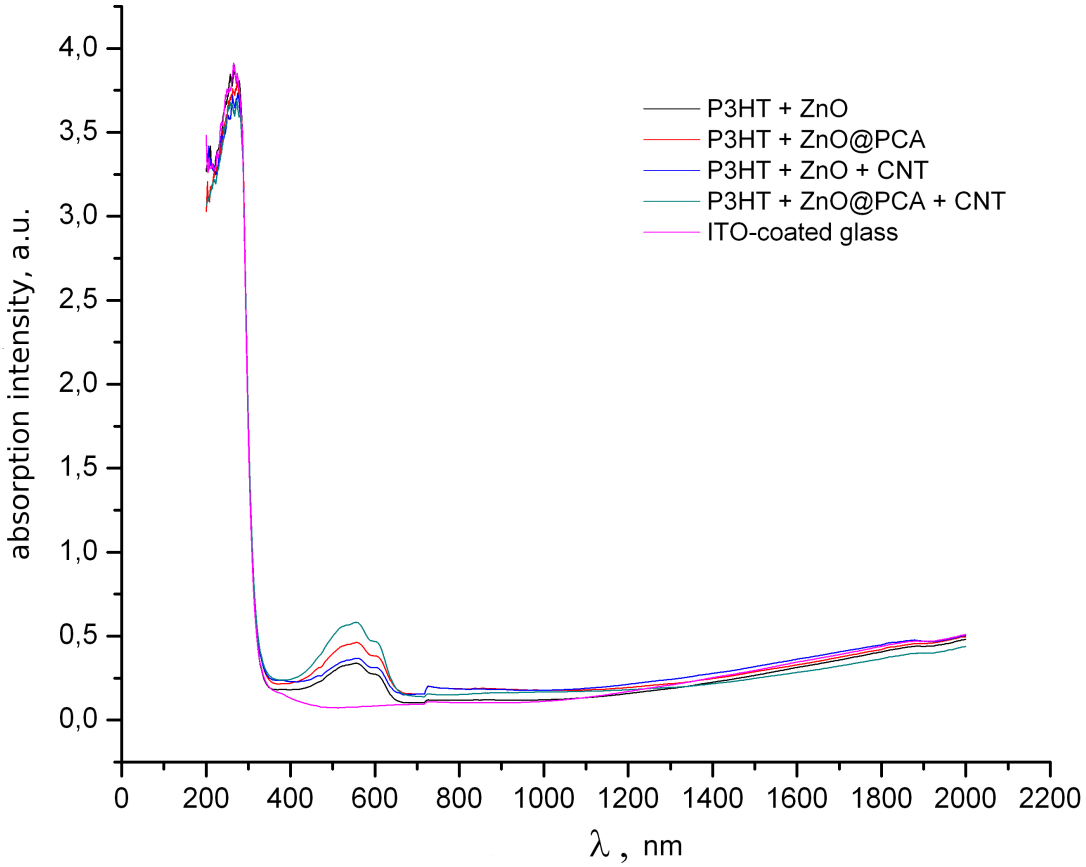

Figure 34. UV-Vis-NIR absorption spectra of the films of active layers on ITO-coated glass.

The most intense band of the spectra (in the UV region below 300 nm) corresponds to the absorption of the substrate; besides, this band also contains the contribution of the absorption of

ZnO, as the bandgap of this semiconductor corresponds to the energy of photons of these wavelengths. The absorption in the IR region is caused by the ITO substrate.
The small distortion around 725 nm is an artefact originated by the switching of the operating light sources / monochromators / detectors during the operation of the spectrometer.

If we compare these spectra with the spectrum of pure P3HT film on glass (figure 35), we can say that the location of the absorption maxima of P3HT (520-560 nm and a shoulder at 600 nm) does not change in the composites (see the detailed section of the spectra in the region of P3HT absorption on figure 35). Though the spectra shown on the figure differ in intensity, reasonable comparison can be done only between the ones with similar values of film thickness, for example: pure P3HT (60 nm), P3HT+ZnO@PCA (60 nm) and P3HT+ZnO@PCA+CNT (87 nm); but not between the thicker and the thinner films due to the big difference in film morphologies. It should be noted that in this case normalisation of the band intensities to a certain common thickness value was performed.

Specifically, modification of P3HT+ZnO@PCA active layer with CNT practically does not bring about any alteration to the intensity or to the position of the absorption band. A slightly higher absorption intensity is observed for the film of pure P3HT. However, this seems to be just the effect of the relative content of P3HT in the films, particularly in the P3HT+ZnO@PCA there is a lower quantity of P3HT than in the film of pure P3HT of the same thickness. And neither increase of absorption caused by the presence of CNT or PCA nor appearance of the bands characteristic for PCA (see figure 24, p.26) is observed in this spectral region. The reason for this can be the relatively low content of PCA chromophores with respect to P3HT.

If we compare the normalised spectra of P3HT+ZnO and P3HT+ZnO+CNT, again, they appear to be very similar, though the difference in intensity may also be a result of the different morphologies and a more significant film thickness difference than in the previous case (the thicknesses are 19 nm and 14 nm, correspondingly). In addition, for the composition P3HT+ZnO+CNT there is a small shoulder on the absorption band which is absent on the spectrum of P3HT+ZnO composite. However, it remains unclear whether it is caused by the interaction of CNT with P3HT or with ZnO.

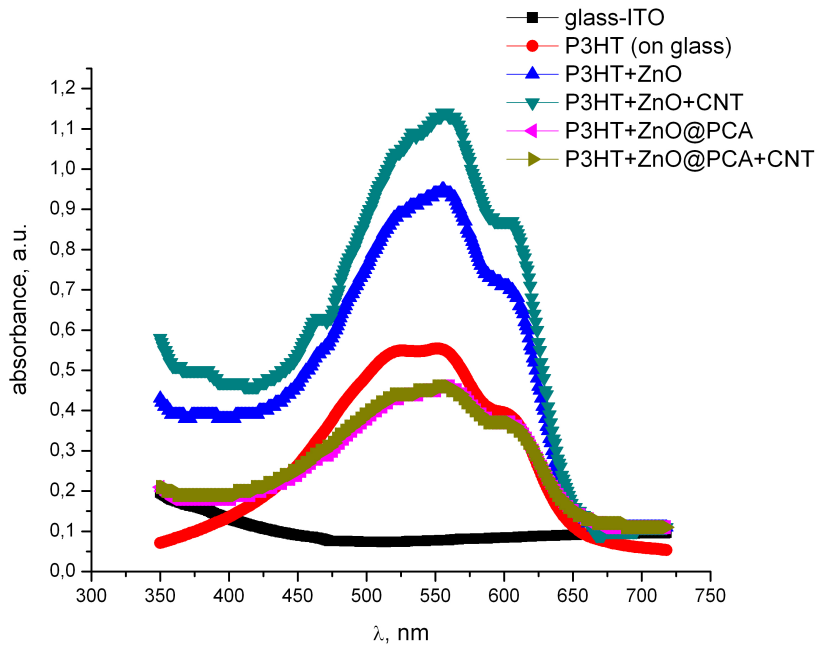

Figure 35. Section of the UV-Vis-NIR absorption spectra of the films of active layers on ITO-coated glass.

4.4. PHOTOLUMINESCENCE SPECTROSCOPY OF THE ACTIVE LAYER MATERIALS

The losses of the energy of light absorbed in the active layer may be either radiative (i.e., via luminescence) or non-radiative (internal conversion into heat). In order to study the radiative losses, the photoluminescence emission spectra of the films of active layers on ITO-coated glass were measured (see figure 36). The wavelength of the excitation light was 450 nm (a value that is close to the maximum of the excitation spectrum of P3HT). All the spectral intensities are normalised according to the thickness of the films.

It can be seen that pure P3HT emits luminescent light with the maxima at about 640 and 680 nm. Addition of ZnO nanoparticles into it increases the intensity of this emission band. And the presence of CNT in the composite leads to a significant increase of the emission. However, in the case of P3HT+ZnO@PCA the addition of CNT does not alter the intensity of the band. Consequently, the modification of ZnO NP with PCA results in the quenching of luminescence in ZnO + CNT composite.

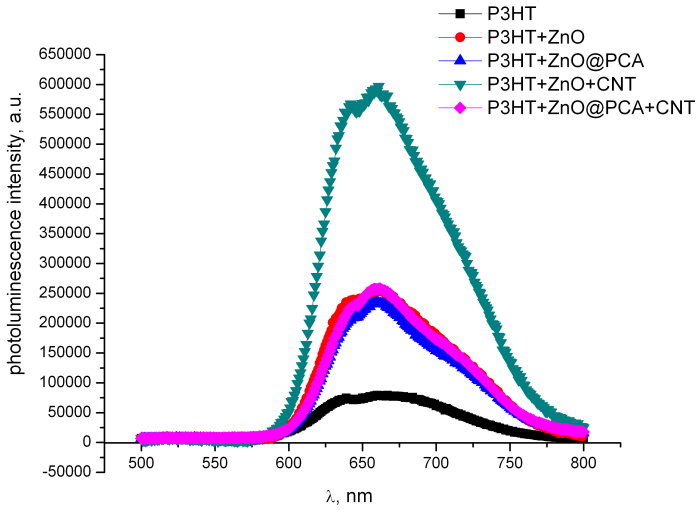

Figure 36. Photoluminescence emission spectra of the active layers on ITO-coated glass; excitation wavelength: 450 nm.

If we consider the photoluminescence emission spectra of the ZnO NP powders (unmodified and modified ones, figure 37), we can see the emission bands with the maximum at about 550 nm for both types of ZnO NP. The PCA-modified ZnO also has a small shoulder on the emission spectrum at about 670 nm that is absent in the unmodified sample. In this case, the comparison of intensities of the bands would be incorrect as different amounts of powders were used for the acquisition of the spectra.

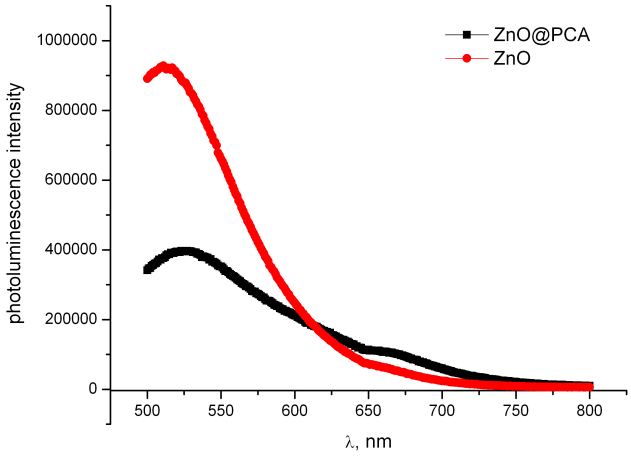

Figure 37. Photoluminescence emission spectra of powders of the unmodified and PCA-modified ZnO nanoparticles; excitation wavelength: 450 nm.

If we compare these spectra with the previously discussed spectra of the P3HT-based active layers, it can be seen that the emission of ZnO in powder samples (550 nm) becomes quenched in the P3HT composites. So one may conclude that in the composites the energy of the light is transferred from ZnO to P3HT and then either results in electric current or is lost via non-radiative recombination or contributes to the luminescence of the polymer.

However, in order to get more representative results, additional experiments need to be conducted, including the comparative photoluminescence studies of ZnO+CNT and ZnO@PCA+CNT composites, as well as the repetition of the measurements which have been done in this work, but with improved morphology of the composite films.

4.5. Solar cell efficiency measurements

At first, direct structure solar cells with single P3HT polymeric active layer were prepared (cell structure Glass/ITO / PEDOT:PSS / P3HT / Al). Current-voltage characteristic of the cell is shown on figure 38. It can be seen that the cell possesses low current density values and does not show any photovoltaic effect.

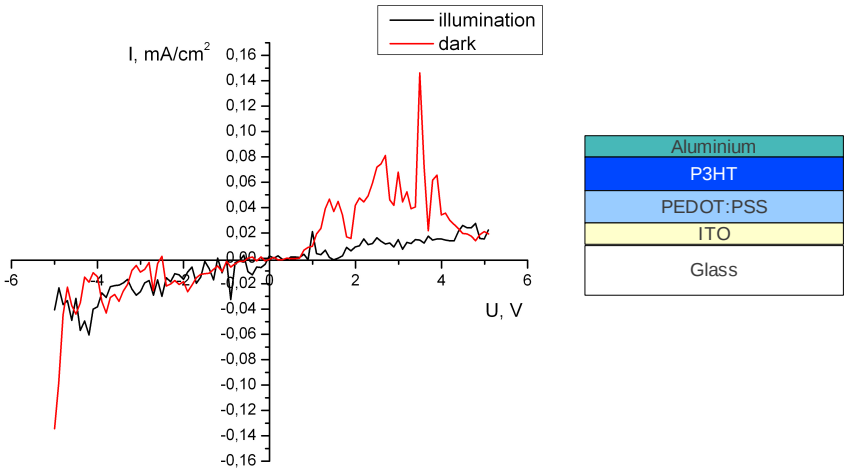

Figure 38. Current-voltage curves of the direct structure solar cell with non-modified P3HT active layer.

In the next series of experiments, modification of the layers of the cell with pristine carbon nanotubes (1% mass with respect to the corresponding polymer) was performed (see the current-voltage curves and the cell structures on figure 39).

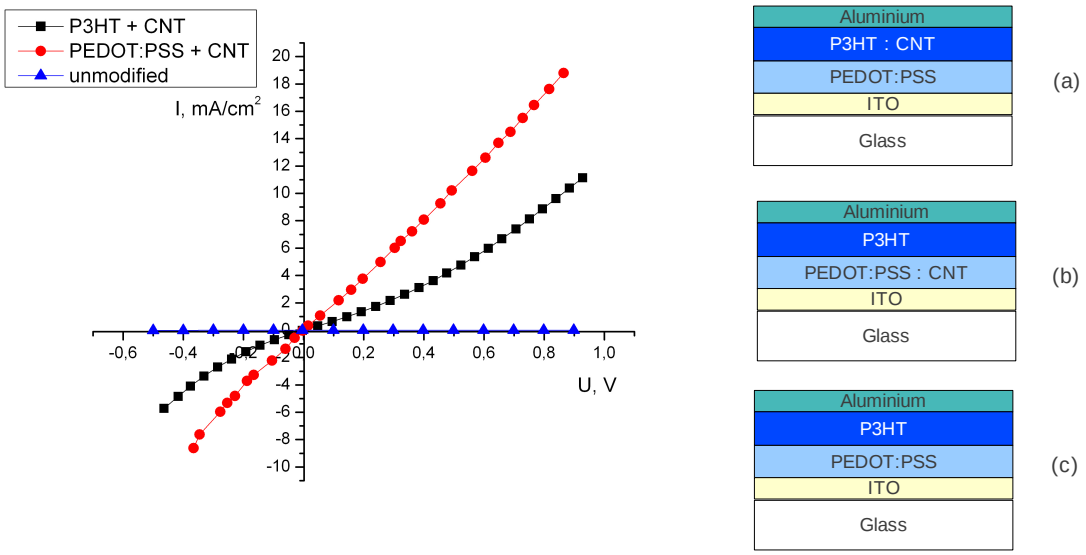

Figure 39. Current-voltage curves of the direct structure solar cells with P3HT-based active layer (under illumination): (a) P3HT with CNT additive; (b) PEDOT:PSS with CNT additive; (c) unmodified.

It can be seen that the addition of CNT leads to substantial increase of the current density, so that the current density of the cell with pure P3HT becomes negligible. However, if we modify the PEDOT:PSS layer, a straight line I-V plot is obtained, typical for an ohmic conductor with a certain resistivity. At the same time, the modification of P3HT leads to a curve, the two halves of which resemble the half of the I-V curve of a diode.

Next the effect of adding the acceptor component (ZnO) to the P3HT was studied using the mass ratio of P3HT to ZnO NP of 10:3. But neither the ZnO NP nor the ZnO@PCA NP (figure 40) brought about any photovoltaic effect, though there is some discrepancy between the curves in the dark and under illumination in both of the cases. However, when taking into consideration the very low values of current density, this effect seems to be negligible. It should be also noted, that the results obtained for the various sections of the same solar cell appear to be different, so the results have pretty bad reproducibility. Most likely, this is caused by the poor morphology of the active layers that was discussed before. Similar morphological problems have been reported in the work performed at our university [9], and in the literature as well [44].

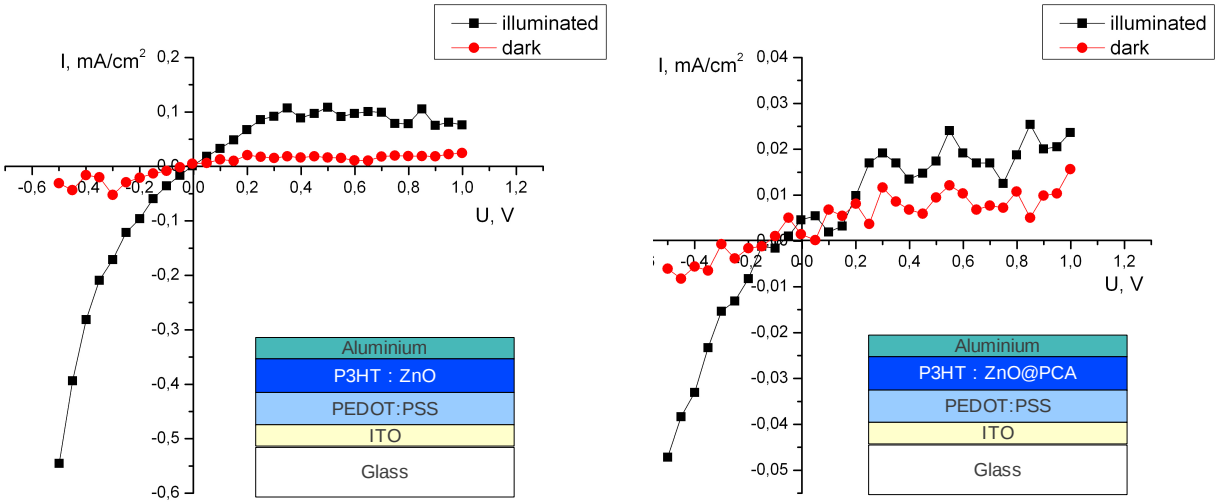

Figure 40. Current-voltage curves and cell structures of the solar cells with P3HT-based active layer: (a) P3HT + ZnO NP (left); (b) P3HT + ZnO@PCA NP (right).

Later, after the polymer was reduced with hydrazine, the preparation of the P3HT + ZnO@PCA cell was repeated, however, no improvements in terms of current density or photovoltaic activity were obtained.

When the concentration of ZnO@PCA in the polymer was significantly increased (up to P3HT : ZnO@PCA mass ratio of 1:2.5), it resulted in the very small photovoltaic effect (see figure 41). However, the current density was, again, extremely low, so the effect that is observed may be considered negligible. From the formal viewpoint, the cell efficiency equalled 0.003% with I_{sc} of about 0.01 mA/cm^2 and U_{oc} of 0.45 V, the fill factor equalled 0.25.

In addition, it should be noted that the high concentration of the poorly dispersed ZnO NP lead to the very rough surface of the active layer as it could be seen visually. However, no specific roughness measurements have been performed because of the time limit.

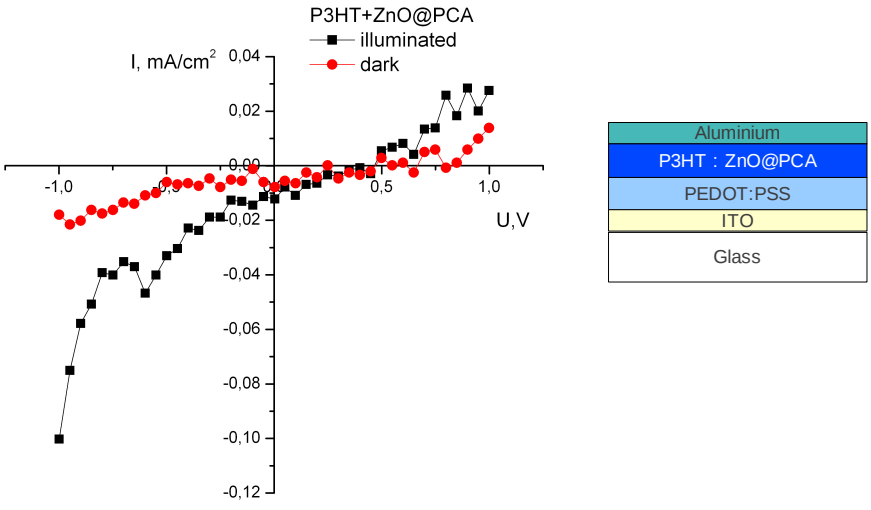

Figure 41. Current-voltage curves and cell structure of the solar cell with P3HT + ZnO@PCA active layer, mass ratio 1:2.5.

If the ZnO@PCA content is further increased (up to P3HT to ZnO@PCA mass ratio of 1:5), even worse surface roughness is obtained. Furthermore, the various types of current-voltage curves were measured for the same sample, including the diode-like behaviour (figure 42, right) and conductor-type one with comparably high current density values (figure 42, left). So the results for this composition are rather non-reproducible due to the morphological problems.

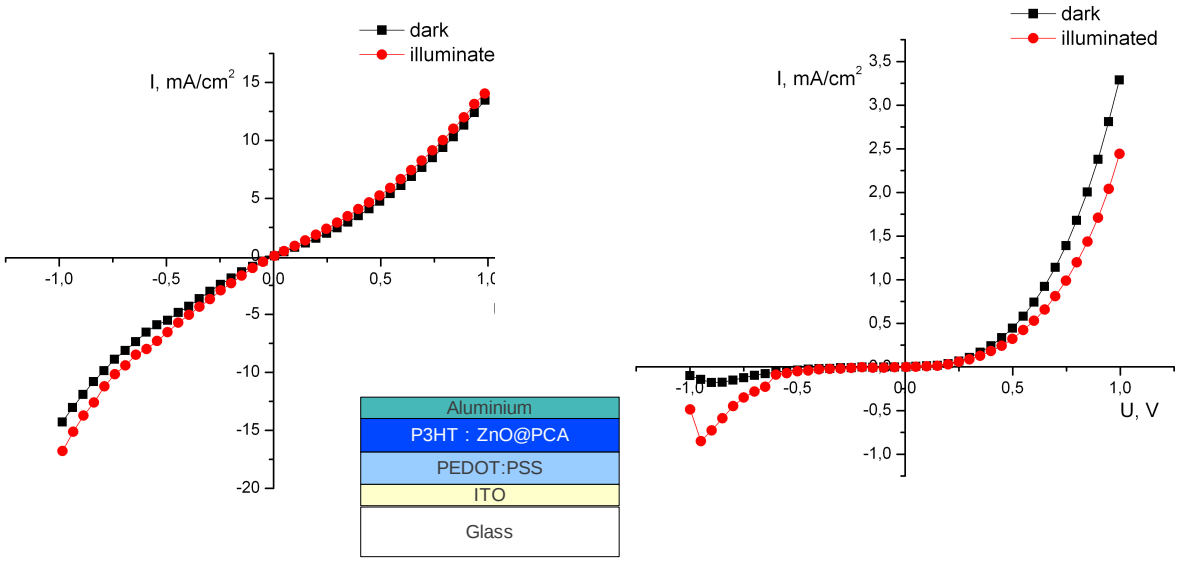

Figure 42. Current-voltage curves and cell structure of variuos sections of the same solar cell with P3HT + ZnO@PCA active layer; mass ratio of P3HT : ZnO@PCA is 1:5.

Afterwards, pristine CNT were added to the P3HT + ZnO NP and P3HT + ZnO@PCA NP active layer suspensions (with the P3HT to ZnO ratios of 10:3). The current-voltage characteristics of the solar cells with the active layers of these compositions are shown on figure 43. In both cases, almost a straight line plot is obtained, suggesting that there is likely to be a short current between the two electrodes due to the presence of the nanotubes. It should be noted that the modification of ZnO with PCA brings about approximately twofold increase of the current density in the CNT-containing solar cell.

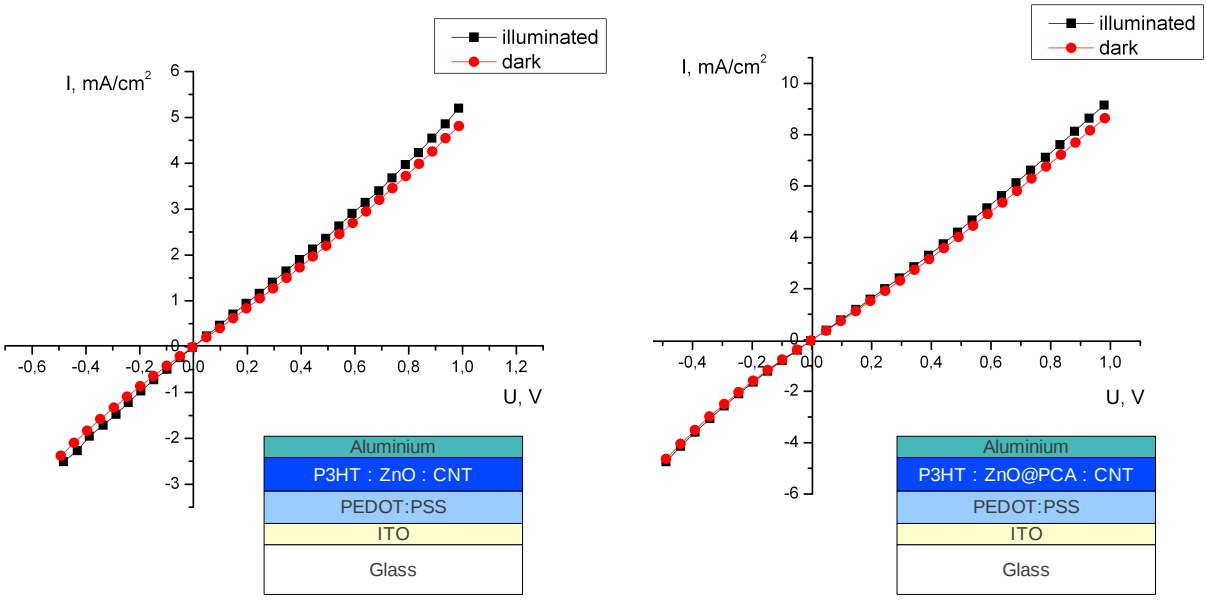

Figure 43. Current-voltage curves and cell structures of the solar cells with P3HT-based active layer: (a) P3HT + ZnO NP + CNT (left); (b) P3HT + ZnO@PCA NP + CNT (right)

A similar result is obtained in the case when CNT are introduced into the P3HT + ZnO@PCA active layer film through the CNT forest transfer process (figure 44), though the current density values are lower than in the previous case. However, the plot looks more straight line-like than before. One can assume that the reason for this effect is that the density of CNT in the active layer and the direct contacts of CNT with both of the electrodes is higher; however, the interaction between P3HT and CNT is weaker which lowers the overall conductivity.

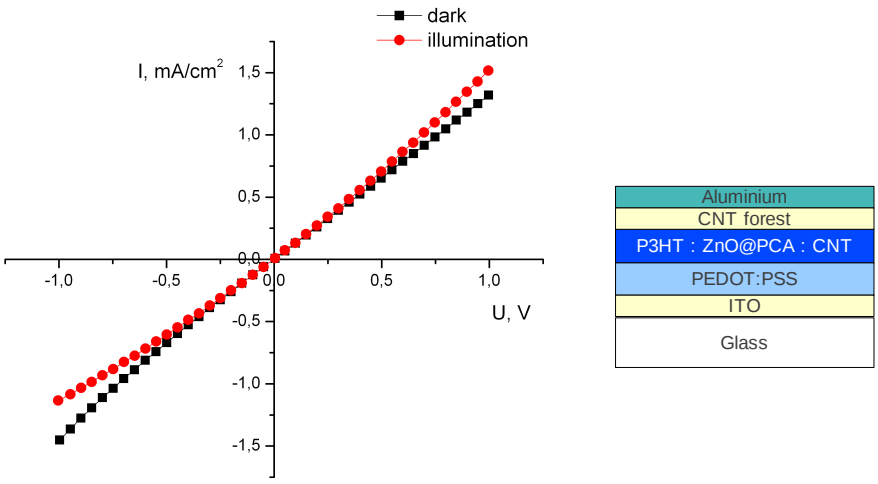

Figure 44. Current-voltage curves and cell structure of the solar cells with the active layer: P3HT + ZnO@PCA + transferred CNT forest

Finally, an attempt was made to prepare 'sandwich' structures from the same solar cell and shorter CNT forest grown on ITO-coated glass (cell structure glass/ITO / PEDOT:PSS / P3HT + ZnO@PCA / CNT forest / ITO/glass). However, this attempt did not succeed because of the low adhesion between the basic cell and the ITO-coated glass with CNT forest on top, so that the two substrates did not hold together.

If we try to analyse the results of the cells preparation and testing, the following possible reasons for the absent or extremely low photovoltaic cell efficiency can be outlined:

- bad morphology of the active layer, including:
  - absence of percolation for ZnO NP (so that they appear to be in closed aggregates rather then as nanoparticles percolation chain);
  - poor dispersion quality of ZnO NP, due to which the bulk heterojuction morphology (required for the 5-10 nm exciton mobility radius of P3HT) is not reached which, in turn, causes significant losses. Though, modification with PCA leads to a slight improvement of the dispersion;

- improper layer sequence, so that there may appear to be a direct contact for one type of material (either donor or acceptor) to both sides of the active layer (i.e., in the direction of the different electrodes) simultaneously. Hence, the charge carriers inside of ZnO may flow to both of the electrodes, so that recombination and no charge separation occurs;

- non-satisfactory properties of the photoactive polymer, including:
  - improper purity grade of the purchased polymer, so that residues of the catalysts used during synthesis may be present, as well as of low-molecular weight fractions which are less conductive. Furthermore, the polymer can possess relatively low regioregularity which is also crucial for its conductivity. In order to avoid this factor, purification procedure should be performed or a more purified substance has to be purchased;
  - oxidation of the polymer that leads to the destruction of the conjugation chain. In the first series of experiments, P3HT that was stored for quite a long period of time under ambient conditions (thus subjected to the influence of oxygen in the air) demonstrated low current density values. The reduction of the sample with hydrazine did not improve these values, so multi-step Soxhlet extraction that is reported in the literature [44] to be used for the purification of the polymer and its fractioning (separation of the most conductive high-molecular fraction) seems to be a reasonable step to do for obtaining polymer with sufficient conductivity. However, due to practical reasons, including low quantity of P3HT sample available, this procedure has not been performed.

    Another issue is storage of the polymer and its processing. In order to avoid any degradation, inert (e.g., nitrogen) atmosphere is crucial. In the optimal case, all the procedures should be done in single specialized room that includes a glovebox under nitrogen atmosphere with access to all the needed equipment: spin-coater, hot plate, evaporation deposition chamber.

- P3HT / ZnO interface quality.

  According to the Raman and IR spectra discussed in 4.1., the unmodified ZnO nanoparticles appear to be surrounded by negatively charged acetate counter-ions. The PCA-modified ZnO NP, in turn, combine both acetate and pyrene-1-carboxylate anions as counter-ions. Important issue is that there is no covalent bonding between the PCA or acetate groups and the surface of ZnO. As a result, the electron-accepting properties that

ZnO possesses due to the position of its band energy levels may be suppressed by the presence of these anions, namely the electrons that should be attracted to the positively charged ZnO surface will be repulsed by them. The only possible way to avoid this effect may be that the anion actually belongs to the donor phase, i.e., when there is a very efficient exciton transfer from P3HT through the anion to the interface between the anion and ZnO surface. In the case of PCA, this can be possible via π-π interaction between pyrene aromatic system and thiophene aromatic rings of P3HT. In fact, the slight improvement of dispersion quality of ZnO@PCA NP when compared to the unmodified ZnO NP suggests that some interaction of this type actually takes place.

However, the acetate anions are unlikely to form any bonding of this type, so they can act only as a Coulomb barrier and cause repulsion of the electrons that could otherwise be withdrawn by ZnO as an acceptor component of the active layer. Taking into consideration the fact that the acetate anions are present both around the unmodified and (partly) around the PCA-modified ZnO NP, this may be the problem for both of the cases.

A similar conclusion can be made from the results obtained in the previous work [9]. The only difference, as it was mentioned before, is that in that work the coordination of ethyl acetate on the surface of the unmodified ZnO NP is reported. However, again, there is no evidence of covalent bonding of the organic groups on the ZnO NP surface.

Regarding the use of carbon nanotubes for the modification of the active layers, it appears that they can improve the conductivity values of a cell significantly, however, there is no preferential interaction between the tubes and the acceptor material (ZnO NP / ZnO FNP), so that CNT have a contact with both donor (P3HT) and acceptor. As a consequence, no charge separation may happen, as CNT are known to be both good electron and hole conductors.

This effect is further increased by the dimensions of the tubes. Even the length of the shortest CNT exceeds the thickness of the active layer. As a consequence, it is very likely that direct contact between the two electrodes is established causing the short-current between them.

5. Conclusions and recommendations

To sum up, an attempt was made to produce hybrid solar cells based on P3HT and zinc oxide nanostructures and also incorporating carbon nanotubes. For this purpose, zinc oxide nanoparticles were synthesized. Additionally, the modification of the nanoparticles with an organic dye was performed. Investigation of the properties and parameters of the materials used in the work was performed, including analysis of the properties of zinc oxide nanostructures and determination of the optical absorption and luminescence properties of the active layers of the solar cells. Separately, CVD growth of CNT forests was performed and the use of aligned CNT forests for the modification of the active layers was attempted.
Finally, the cells were prepared and their current-voltage characteristics were measured.

The work did not result in the achievement of any satisfactory efficiency of a solar cell. However, beside the practical experience gained during it, some recommendations can be made regarding the materials that were investigated.

First of all, if there is an aim of creating an efficient excitonic solar cell using ZnO nanostructures as an acceptor component, different conducting polymers and modifying dyes need to be applied in order to get bigger spectrum coverage than the one studied in this work.
Another issue is the energy level design of a cell. Within the materials that were used in this work (according to the literature evidence) there is a little barrier for the electron transport between the conduction band of ZnO and the work function of aluminium that can cause resistive losses. However, this does not seem to be the major reason for the absence of solar cell efficiency as some efficiency (0.9%) is reported [44] for the cells with ZnO/Al interface.

In addition, the quality of the conducting polymer used for the preparation of solar cells needs to be controlled, including molecular weight, regioregularity and purity. These properties eventually determine the conductivity of the polymer that should be as high as possible.
A lot of attention should be paid to the storage and handling conditions of the polymer. Most of the common conducting polymers degrade when exposed to ambient air, consequently, inert atmosphere (for example, a nitrogen-filled glove box) has to be assured for the preparation (weighing, dissolving), deposition (spin-coating, evaporation deposition) and annealing steps. Moreover, the sealing of the ready cell with transparent polymeric film seems to be a good idea for providing long-term stability of the cell, if the investigation of cell degradation is also of interest.

Next issue that is crucial for the performance of the hybrid solar cell is the morphology of the active layer. It needs to be significantly improved in order to get high interfacial area between the donor and the acceptor phases; at the same time, percolation of the nanoparticles needs to be present in order for the charge carriers to be efficiently conducted to the corresponding electrode.

In the case that direct mixing of the ready solutions of the donor and the acceptor is used for the preparation of the suspension of the active layer material, dispersion quality of the ZnO NP is a crucial issue. The use of PCA-type dye as a surface modifier seems to remain a good idea for its improvement. However, the covalent bonding of the dye to ZnO has to be assured in order to avoid any barriers for the charge transfer through the interface between the donor and acceptor phases. Such a barrier is likely to exist if the modifier of the NP is an anion.

As an alternative, the modification of the NP with a dye can be performed in situ during the synthesis of the NP, or even the NP can be synthesised in the solution of the conducting polymer and the dye. This might be an idea towards the good dispersion of the NP in the polymer matrix. However, special care should be taken in order to avoid any damage to the polymer.

Regarding the use of carbon nanotubes for the modification of the active layer of the hybrid solar cells, this still seems to be a prospective idea because of the significant effect of CNT on conductivity improvement of the conductive polymer and of the dye-modified ZnO / polymer composites. However, improper contact sequence (i.e., contacting of CNT with both the conducting polymer and ZnO NP at the same time) may lead to the recombination of the opposite charge carriers (electrons and holes) in the region of the nanotubes. As a result, no charge separation and preferential charge conductivity may occur, hence no photovoltaic effect can be observed. And this effect is further increased by the big relative length of the tubes that allows them to penetrate through all of the layers of the cell and create a percolation that leads to a short current between the two electrodes of the solar cell.

Consequently, if CNT will be tuned so that they are attached exclusively to one of the active layer materials (either donor or acceptor), but not to another one, the effect of CNT on conductivity is likely to boost the solar cell performance. And, of course, the contact has to be established only with one of the electrodes, so the tubes need to have a tilted alignment, be relatively short or the active layer thickness has to be increased.

From this viewpoint, an interesting way of the generation of the active layer of a cell could be the polymerisation of the conducting polymer directly from the surface of carbon nanotubes, followed by the addition of the acceptor component.

6. REFERENCES

[1] M. Pagliaro, G. Palmisano, and R. Ciriminna, Flexible solar cells, WILEY-VCH Verlag GmbH & Co. KGaA, Weinheim (2008).

[2] S. Kurtz, Opportunities and challenges for development of a mature concentrating photovoltaic power industry, NREL Technical Report (November 2009).

[3] F. C. Krebs, Roll-to-roll fabrication of monolithic large-area polymer solar cells free from indium-tin-oxide, Solar Energy Materials & Solar Cells 93 (2009) 1636–1641.

[4] http://www.pv-tech.org/news/_a/solarmer_breaks_organic_solar_pv_cell_conversion_efficiency_record_hits_nre (accessed on September, 12th).

[5] M. Skompska, Hybrid conjugated polymer/semiconductor photovoltaic cells, Synthetic Metals 160 (2010) 1–15.

[6] http://blog.disorderedmatter.eu/2008/06/05/picture-story-how-do-organic-solar-cells-function (accessed on September, 12th).

[7] H.-Y. Chen, Polymer solar cells with enhanced open-circuit voltage and efficiency, Nature Photonics vol. 3 (2009), DOI: 10.1038/NPHOTON.2009.192.

[8] L. Tsakalakos, Nanostructures for photovoltaics, Materials Science and Engineering R 62 (2008) 175–189.

[9] B. A. Gonfa, Fabrication of solar cells from poly(3-hexylthiophene) and ZnO nanostructures, MSc thesis, University of Aveiro, Portugal (2009).

[10] T. Zdanowicz, T. Rodziewicz, M. Zabkowska-Waclawek, Theoretical analysis of the optimum energy band gap of semiconductors for fabrication of solar cells for applications in higher latitudes locations, Solar Energy Materials & Solar Cells 87 (2005) 757–769.

[11] E. Bundgaard, F.C. Krebs, Low band gap polymers for organic photovoltaics, Solar Energy Materials & Solar Cells 91 (2007) 954–985.

[12] A. J. Nozik, Multiple exciton generation in semiconductor quantum dots, Chemical Physics Letters 457 (2008) 3–11.

[13] M. Jørgensen, K. Norrman, F. C. Krebs, Stability/degradation of polymer solar cells, Solar Energy Materials & Solar Cells 92 (2008) 686–714.

[14] N. Tomczak, D. Jańczewski, M. Han, G. J. Vancso, Designer polymer–quantum dot architectures, Progress in Polymer Science 34 (2009) 393–430.

[15] L. H. Jimison, J. Rivnay, M. F. Toney, A. Salleo, Microstructure, charge transport and trapping in anisotropic polymeric thin film transistors, Digest of the IEEE/LEOS summer topical meetings (2007) 206-207.

[16] Z. Spitalsky, D. Tasis, K. Papagelis, C. Galiotis, Carbon nanotube – polymer composites: Chemistry, processing, mechanical and electrical properties, Progress in Polymer Science 35 (2010) 357–401.

[17] A. W. Musumeci, MWNT polymer nanocomposites based on P3HT, Advanced Materials Research Vols. 29-30 (2007) 291-294.

[18] A. W. Musumeci, G. G. Silva, J.-W. Liu, W. N. Martens, E. R. Waclawik, Structure and conductivity of multi-walled carbon nanotube/poly(3-hexylthiophene) composite films, Polymer 48 (2007) 1667-1678.

[19] B. J. Landi, S. L. Castro, H. J. Rufa, C. M. Evansa, S. G. Bailey, R. P. Raffaelle, CdSe quantum dot-single wall carbon nanotube complexes for polymeric solar cells, Solar Energy Materials & Solar Cells 87 (2005) 733–746.

[20] S. Chaudhary, Hierarchical placement and associated optoelectronic impact of carbon nanotubes in polymer-fullerene solar cells, Nano Letters Vol. 7 (2007), No. 7 1973-1979.

[21] C. D. Canestraro, M. C. Schnitzler, A. J. G. Zarbin, M. G. E. da Luz, L. S. Roman, Carbon nanotubes based nanocomposites for photocurrent improvement, Applied Surface Science 252 (2006) 5575–5578.

[22] M.-C. Wu, Y.-Y. Lin, S. Chen, H.-C. Liao, Y.-J. Wu, C.-W. Chen, Y.-F. Chen, W.-F. Su, Enhancing light absorption and carrier transport of P3HT by doping multi-wall carbon nanotubes, Chemical Physics Letters 468 (2009) 64–68.

[23] C. Li, Y. Chen, Y. Wang, Z. Iqbal, M. Chhowallab, S. Mitra, A fullerene–single wall carbon nanotube complex for polymer bulk heterojunction photovoltaic cells, J. Mater. Chem., 17 (2007) 2406–2411.

[24] E. Kymakis, N. Kornilios, E. Koudoumas, Carbon nanotube doping of P3HT:PCBM photovoltaic devices, J. Phys. D: Appl. Phys. 41 (2008) 165110.

[25] S. Berson, R. de Bettignies, S. Bailly, S. Guillerez, B. Jousselme, P3HT/CNT/PCBM composites for organic photovoltaic cells, Adv. Funct. Mater. 17 (2007) 3363–3370.

[26] T. Schuettfort, H. J. Snaith, A. Nish, R. J. Nicholas, Synthesis and spectroscopic characterization of solution processable highly ordered polythiophene–carbon nanotube nanohybrid structures, Nanotechnology 21 (2010) 025201.

[27] J. Geng, B.-S. Kong, S. B. Yang, S. C. Youn, S. Park, T. Joo, H.-T. Jung, Electron transfer properties of P3HT/SWNT hybrids, Adv. Funct. Mater. 18 (2008) 2659–2665.

[28] J. Arranz-Andrés, W. J. Blau, Enhanced device performance using different carbon nanotube types in polymer photovoltaic devices, Carbon 46 (2008) 2067–2075.

[29] R. Ulbricht, S. B. Lee, X. Jiang, K. Inoue, M. Zhang, S. Fang, R. H. Baughman, A. A. Zakhidov, Transparent carbon nanotube sheets as 3-D charge collectors in organic solar cells, Solar Energy Materials & Solar Cells 91 (2007) 416–419.

[30] T. Umeyama, H. Imahori, Carbon nanotube-modified electrodes for solar energy conversion, Energy Environ. Sci., 1 (2008) 120–133.

[31] A. J. Miller, R. A. Hatton, S. R. P. Silva, Interpenetrating multiwall carbon nanotube electrodes for organic solar cells, Applied Physics Letters 89 (2006) 133117.

[32] A. Du Pasquier, H. E. Unalan, A. Kanwal, S. Miller, M. Chhowalla, Conducting and transparent single-wall carbon nanotube electrodes for polymer-fullerene solar cells, Appl. Phys. Lett. 87 (2005) 203511.

[33] E. Kymakis, E. Stratakis, E. Koudoumas, Integration of carbon nanotubes as hole transport electrode in polymer/fullerene bulk heterojunction solar cells, Thin Solid Films 515 (2007) 8598–8600.

[34] R. Ulbricht, X. Jiang, S. Lee, K. Inoue, M. Zhang, S. Fang, R. Baughman, A. Zakhidov, Polymeric solar cells with oriented and strong transparent carbon nanotube anode, Phys. Stat. Sol. (b) 243 No.13 (2006) 3528-3532.

[35] R. A. Hatton, N. P. Blanchard, L. W. Tan, G. Latini, F. Cacialli, S. Ravi, P. Silva, Oxidised carbon nanotubes as solution processable, high work function hole-extraction layers for organic solar cells, Organic Electronics 10 (2009) 388–395.

[36] J. Zou, L. Liu, H. Chen, S. I. Khondaker, R. D. McCullough, Q. Huo, L. Zhai, Dispersion of pristine carbon nanotubes using conjugated block copolymers, Adv. Mater. 20 (2008) 2055–2060.

[37] S. Huang, Patterned growth and contact transfer of well-aligned carbon nanotube films, J. Phys. Chem. B 103 (1999) 4223-4227.

[38] H. T. Ng, Growth of carbon nanotubes: a combinatorial method to study the effects of catalysts and underlayers, J. Phys. Chem. B 107 (2003) 8484-8489.

[39] Z. L. Wang, ZnO nanowire and nanobelt platform for nanotechnology, Materials Science and Engineering R 64 (2009) 33–71.

[40] L. Schmidt-Mende, J. L. MacManus-Driscol, ZnO – nanostructures, defects, and devices, Materials Today, vol. 10 No. 5 (2007) 40-48.

[41] A. I. Hochbaum, P. Yang, Semiconductor nanowires for energy conversion, Chem. Rev. 110 (2010) 527–546.

[42] A. B. Djurišić, A. M. C. Ng, X. Y. Chen, ZnO nanostructures for optoelectronics: Material properties and device applications, Progress in Quantum Electronics 34 (2010) 191–259.

[43] K. Kim, B. Jung, J. Kim, W. Kim, Effects of embedding non-absorbing nanoparticles in organic photovoltaics on power conversion efficiency, Sol. Energy Mater. Sol. Cells (2010), doi:10.1016/j.solmat.2010.05.049.

[44] W. J. E. Beek, M. M. Wienk, R. A. J. Janssen, Solar cells from P3HT and ZnO nanoparticles, Adv. Funct. Mater. 16 (2006) 1112–1116.

[45] M. Wang, X. Wang, P3HT/ZnO bulk-heterojunction solar cell sensitized by a perylene derivative, Solar Energy Materials & Solar Cells 92 (2008) 766–771.

[46] M. M. Stylianakis, J. A. Mikroyannidis, E. Kymakis, A facile, covalent modification of single-wall carbon nanotubes by thiophene for use in organic photovoltaic cells, Solar Energy Materials & SolarCells 94 (2010) 267–274.

[47] J. A. Mikroyannidis, M. M. Stylianakis, P. Suresh, G.D. Sharma, Efficient hybrid bulk heterojunction solar cells based on phenylenevinylene copolymer, perylene bisimide and TiO_2, Solar Energy Materials & Solar Cells 93 (2009) 1792–1800.

[48] D. A. Schwartz, N. S. Norberg, Q. P. Nguyen, J. M. Parker, D. R. Gamelin , Magnetic quantum dots: synthesis, spectroscopy, and magnetism of Co^{2+}- and Ni^{2+}-doped ZnO nanocrystals, J. Am. Chem. Soc. 125 (2003) 13205-13218.

[49] D. Liu, W. Wu, Y. Qiu, S. Yang, S. Xiao, Q.-Q. Wang, L. Ding, J. Wang , Surface functionalization of ZnO nanotetrapods, Langmuir Vol. 24 No. 9 (2008) 5053.

[50] A. V. Ghule, B. Lo, S.-H. Tzing, K. Ghule, H. Chang, Y. C. Ling , Simultaneous thermogravimetric analysis and in situ thermo-Raman spectroscopic investigation of thermal decomposition of zinc acetate dihydrate forming zinc oxide nanoparticles, Chemical Physics Letters 381 (2003) 262–270.

[51] K. Ananthanarayanan, Raman spectra of single crystals of Zn & Li acetates dihydrates, Proc. Ind. Acad. Sci. A vol. LVI (1962) Pl. VI.

[52] H. Geng, Y. Guo, R. Peng, S. Han, M. Wang, A facile route for preparation of conjugated polymer functionalized inorganic semiconductors and direct application in hybrid photovoltaic devices, Solar Energy Materials & Solar Cells 94 (2010) 1293–1299.

ANNEX

Figure 45. Photograph of the home-constructed glovebag

Figure 46. Photograph of the home-constructed heating plate